Institute of Hydrology

Natural
Environment
Research
Council

Rainfall forecasting using a simple advected cloud model with weather radar, satellite infra-red and surface weather observations: An initial appraisal under UK conditions

by

V.A. BELL, D.S. CARRINGTON AND R.J. MOORE

Executive Summary

A simple two-dimensional rainfall model, based on advection and conservation of mass in a vertical cloud column, is investigated for use in real-time rainfall forecasting for flood warning. The model is capable of assimilating data from weather radar, infra-red satellite and surface weather observations to obtain frequently updated forecasts which help compensate for the simplified model dynamics. A development of the model for UK conditions employs radar scan data for four elevations on a 5 km grid. Multiquadric interpolation is used to map these data onto a regular 84 by 84, 5 km grid in the horizontal and 15, 1 km intervals in the vertical. These interpolated data provide estimates of the vertically integrated liquid water content of the cloud column associated with each radar pixel for assimilation into the model.

The model is assessed using data for the Wardon Hill radar in southern England for the period 8 to 12 June 1993 when a number of thunderstorms occurred over southern Britain. Five model variants are considered ranging from simple persistence and advection methods, used as a baseline, to forms of the dynamic rainfall model solved in different ways. A full numerical solution of the nonlinear dynamic model most often provides the best forecasts. However, for convective storms the model seriously overestimates rainfall intensities. This points to the need to improve the estimation of liquid water content in each cloud column, and its conversion back to rain. A number of recommendations for further work are given.

Acknowledgements

Contents

1. Introduction

Simple advection methods based on weather radar provide a practical means of forecasting rainfall fields in real-time out to two to six hours in support of storm and flood warning. The velocity and direction of storm movement may be obtained either from a mesoscale model (Brown *et al.*, 1994) or from weather radar images displaced in time (Moore *et al.*, 1991, 1992). Forecast fields are then obtained by advecting the current radar image forwards in time according to this trajectory, possibly with some modification. Such forecasts can be formed on a 2 km or 5 km grid as 15 minute rainfall totals and updated every 15 or 30 minutes. These methods, however, fail to perform adequately when there is development of the rainfall field, in spatial extent and/or intensity, or when changes in the storm trajectory occur. Whilst the latter may be less important for forecasting over restricted catchment areas and for the shorter lead times of primary interest to hydrologists, development of the rainfall field can be a major cause of poor advection forecasts, particularly for convective storms. Attempts to model development by inference from time-displaced radar images has generally led to less reliable forecasts (Moore *et al.*, 1991).

Physically-based approaches to rainfall forecasting provide an obvious alternative. However, the current generation of mesoscale model (Golding, 1990) represent storm dynamics on too coarse a grid to meet the hydrologists' needs - 16 km in the case of the UK Met. Office Mesoscale Model - with highly parameterised representations, for example, of convective cloud systems. Even if mesoscale models proved highly reliable at forecasting rainfall amounts their coarse grid scale would fail to meet the hydrological requirement for catchment scale rainfall, at least for the more spatially variable convective storms or for the smaller catchments of particular interest in urban areas. Disaggregation of mesoscale model rainfall to smaller scales provides one possible approach. However, an interesting alternative is to pursue the physics-based approach at a smaller scale and higher level of process representation. An extreme approach would be to employ one of the number of detailed cloud models (Smolarkiewicz & Clark, 1985) currently developed to support phenomenological studies of precipitation formation. However, in the development of an operational rainfall forecasting model it is important that the complexity of the model formulation is commensurate with the observation data available for assimilation into the model. This argument leads one to consider simple model parameterisations which encapsulate the dominant dynamics affecting precipitation formation. One such model, which stems from the work of Kessler (1969), Georgakakos and Bras (1984) and Seo and Smith (1992), is the Iowa Rainfall Model of French and Krajewski (1994). It is a simple two-dimensional rainfall model based on the conservation of mass in a vertical cloud column. Since the model is essentially a simple dynamic water balance of the lower atmosphere it has much in common with the conceptual catchment water balance models familiar to hydrologists working in the land phase of the hydrological cycle. Using a rainfall model parameterisation commensurate with that of a catchment model clearly has much to commend it for the purposes of storm and flood forecasting. Depending on the resolution of the radar data the model is capable of modelling rainfall fields for 1, 2 or 5 km grids and for time intervals of from 5 to 15 minutes, for example. It therefore meets the hydrologist's requirement for forecasts at this fine resolution in space and time.

The work reported here outlines the changes made to the Iowa Rainfall model to adapt it for use with UK weather radar and satellite data, and then evaluates the model's performance for events in the period 9-12 June 1993. Sections 2 and 3 provide a derivation of the governing

1

model equations, and outline the parameterisation used to rewrite these equations in terms of measurable meteorological quantities. Section 4 describes changes made to the model and outlines alternative model formulations evaluated alongside the original Iowa model. Two of these model forms are simplifications of the full model scheme, and are designed to test how each increase in model complexity affects forecast accuracy. The Iowa model was originally developed for use with data from the USA for a radar scanning at 12 elevations. It has been adapted for use with data from the UK for radars scanning at four elevations. This has involved the use of a multiquadric interpolation scheme which places the irregular UK data onto a regular 5 km grid with 15 values in the vertical direction. Details of this scheme and incorporation of other data are outlined in Section 5. The forecast results are given in Section 6 for the different model variants at various lead times up to 1 hour ahead. Finally, the overall model performance is discussed in Section 7. A number of recommendations are made for changes in the model that could lead to improvements in forecast accuracy.

2. Model Derivation

The rainfall forecasting model incorporates both advective and convective dynamics in the form of a two dimensional grid-based horizontal advection scheme coupled with conservation of liquid water in the vertical cloud column associated with each radar grid square. A derivation of the model dynamical equations is given below. This follows the derivation given by Seo and Smith (1992) and French and Krajewski (1994). Figure 2.1 provides a schematic of a vertical cloud column in the model serving to clarify the notation introduced below.

The model dynamical equations are derived from the continuity equations of atmospheric water:

$$
\begin{aligned}
\frac{\partial M}{\partial t} + \frac{\partial}{\partial x}(Mu) + \frac{\partial}{\partial y}(Mv) + \frac{\partial}{\partial z}\left(M(w - W_T)\right) &= \Delta W_c \\
\frac{\partial m}{\partial t} + \frac{\partial}{\partial x}(mu) + \frac{\partial}{\partial y}(mv) + \frac{\partial}{\partial z}(mw) &= \Delta Q_c - \Delta W_c \\
\frac{\partial Q}{\partial t} + \frac{\partial}{\partial x}(Qu) + \frac{\partial}{\partial y}(Qv) + \frac{\partial}{\partial z}(Qw) &= -\Delta Q_c \\
\frac{\partial \rho}{\partial t} + \frac{\partial}{\partial x}(\rho u) + \frac{\partial}{\partial y}(\rho v) + \frac{\partial}{\partial z}(\rho w) &= 0
\end{aligned}
\tag{2.1}
$$
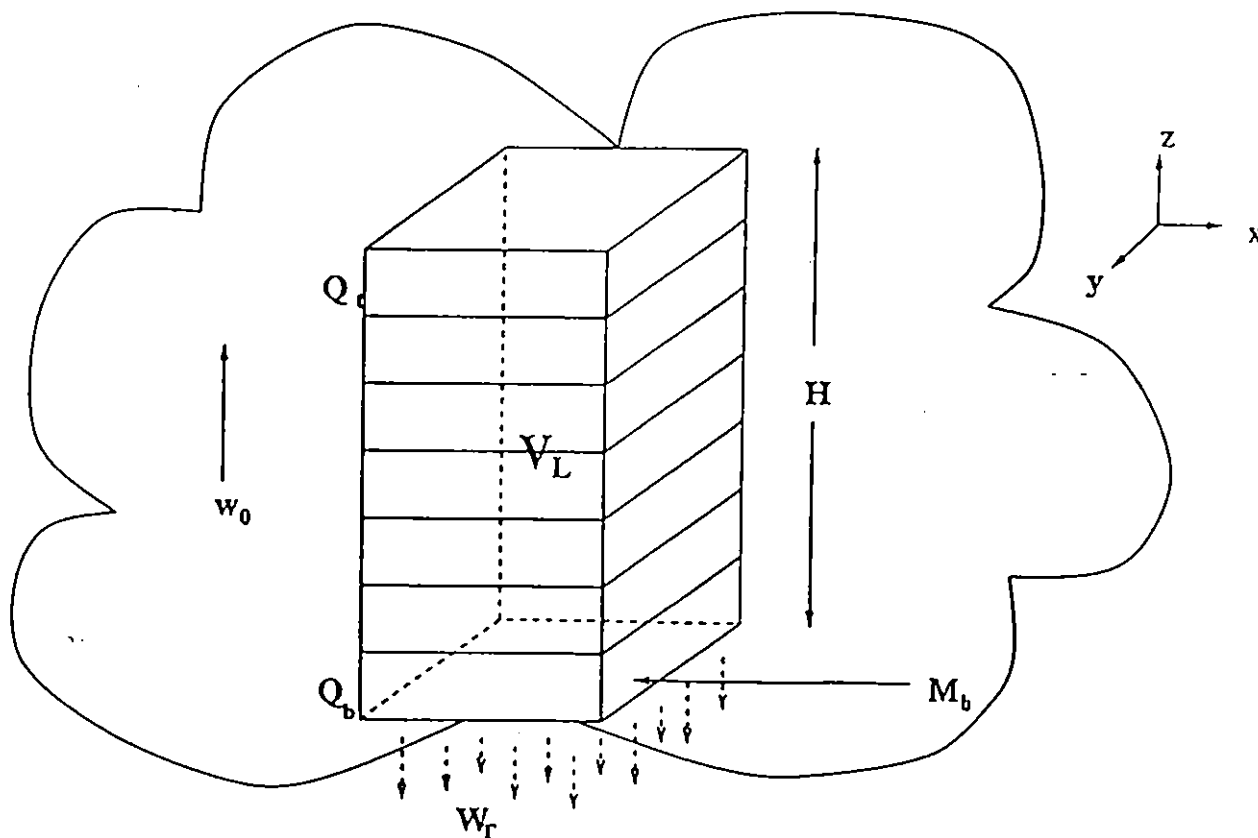
Figure 2.1 Schematic of a vertical cloud column in the dynamic rainfall model

3

where M is rainwater content, m is cloudwater content, Q represents saturation water vapour density and ρ is the density of dry air. The quantities u, v and w represent the horizontal and vertical components of velocity in the x, y and z directions and W_T is the terminal velocity of free falling rain in still air. The terms on the right hand side, ΔW_c and ΔQ_c, are source terms representing, respectively, the conversion of cloud to rain, and the process of condensation to liquid water vapour.

Under the assumption of incompressible air these equations reduce to the set

$$\frac{DM}{Dt} - \frac{\partial}{\partial z}(MW_T) = -\frac{Dm}{Dt} + \Delta Q_c$$

$$\frac{DQ}{Dt} = \Delta Q_c .$$

(2.2)

The operator D/Dt is the total derivative given by the sum of the local derivative with respect to time $\partial/\partial t$ and the convective derivative $\underline{v} \nabla$, where $\underline{v} = $ (u v w) and $\nabla = (\partial/\partial x \;\; \partial/\partial y \;\; \partial/\partial z)^T$; that is

$$D/Dt = \frac{\partial}{\partial t} + \underline{v} \nabla .$$

(2.3)

Although the equations in (2.2) are simple in appearance they are still difficult to model in practice because weather radar is unable to distinguish between cloud water and rain water. The problem is circumvented by making the assumption that on condensation, water vapour turns to rainwater without going through the cloud water phase. This may be interpreted to mean that cloud water is uniform in time and space, i.e. Dm/Dt = 0. A further approximation is made by taking saturation vapour density to be horizontally uniform and locally steady so that DQ/Dt → $w\partial Q/\partial z$.

Finally using a Lagrangian frame of reference (a frame of reference following the motion of the cloud) and implementing the above assumptions gives

$$\frac{\partial M}{\partial t} = -w\frac{\partial M}{\partial z} + \frac{\partial}{\partial z}(MW_T) - w\frac{\partial Q}{\partial z} .$$

(2.4)

Integrating over the height of the cloud from the bottom, z_b, to the top, z_t, under the assumption of constant vertical velocity w over the forecast lead time (necessary because the vertical momentum equation is not included in the model), results in the following equation for the rate of change of cloud water content in time for each vertical cloud column:

$$\frac{dV_L}{dt} = w_o(Q_b - Q_t) - (W_T - w_o)M_b$$

(2.5)

where $V_L(t)$ is the vertically integrated liquid water content

$$V_L(t) = \int_{z_b}^{z_t} M dz .$$

(2.6)

This equation incorporates the boundary condition of zero rainwater at the cloud top and the

4

assumption that the free fall velocity of water is constant up the height of the cloud, i.e. $\partial W_T/\partial z = 0$. The equation represents a mass balance equation expressing the change in cloud water content as the difference between the inflow of water between z_b and z_t, and the outflow via rain from the cloud base.

The assumption of constant vertical velocity might, in future versions of the model, be changed to accommodate a vertical equation of motion. This could be particularly beneficial in the case of convective storms. A simpler alternative might be to implement a piecewise linear distribution for velocity similar to that suggested by Georgakakos & Bras (1984a).

3. Model Parameterisation

3.1 INTRODUCTION

With the aim of practical rainfall forecasting, the mass balance equation (2.5) is parameterised so that the unknown variables - the vertically integrated water content V_L, updraft velocity w_o, vapour density Q, and the rainfall velocity at the cloud base W_T - are expressed in terms of measurable quantities such as weather radar, satellite and ground-based climate measurements.

The following summarises the parameterisation employed by French and Krajewski (1994) in their forecasting model, and outlines the main differences between their model, and a related model outlined in Seo and Smith (1992). Both authors implement very similar parameterisations to estimate the quantity $(W_T - w_o)$, the velocity of rain at the cloud base, and the saturation water vapour densities at the cloud top and base, Q_T and Q_b. The main differences between the two modelling approaches is in the estimation of the updraft velocity w_o and the rainwater content at the cloud base, M_b.

3.2 VELOCITY OF RAINFALL AT THE CLOUD BASE

The quantity $W_T - w_o$ in the mass balance equation represents the velocity of rainfall at the cloud base, i.e. $\nu_b = W_T - w_o$. It is estimated from variables such as the drop-size distribution (Marshall Palmer, 1948) and an expression for the terminal velocity of rain given by Atlas and Ulbrich (1977). The resulting expression for ν_b is given by

$$\nu_b = \Lambda^{-\beta} \frac{\alpha}{6} \Gamma(4+\beta) - w_o = \{M_b/(\pi \rho_o N_o)\}^{\gamma} \frac{\alpha}{6} \Gamma(4+\beta) - w_o \tag{3.1}$$

where M_b is the liquid water content at the cloud base, ρ_o is water density, Λ and N_o are dropsize distribution parameters, $\Gamma(\ )$ is the Gamma function and α and $\gamma = \beta/4$ are dimensionless empirical parameters. A derivation of equation (3.1) is given in Appendix I.

3.3 SATURATION WATER VAPOUR DENSITIES

Saturation water vapour densities Q_b and Q_t are given by

$$Q(z,t) = \frac{r_s(T(z),p(z))p(z)}{R_d T(z)} \tag{3.2}$$

applied at the cloud top and bottom. Here T(z) is the cloud temperature, p(z) is the pressure, r_s is the saturation mixing ratio of air with water and R_d is the specific gas constant for dry air. Temperature and pressure at the cloud base are estimated from surface observations using Parcel Theory (see, for example, Wallace and Hobbs 1977, Rogers and Yau 1985). The temperature at the cloud top T_t is obtained from infra-red satellite imagery. Pressure at the cloud top, p_t, is obtained by solving the following expression for the equivalent potential temperature:

$$\theta_e = T_i \left[\frac{p_n}{p_i} \right]^\kappa \exp \left[\frac{L(T_i) r_s(T_i, p_i)}{c_p T_i} \right] \tag{3.3}$$

where the exponent $\kappa = R_d/c_p = 0.286$, $p_o = 1000$ mb, L is the latent heat of condensation, and c_p is the specific heat of dry air at constant pressure. Further details of the Parcel Theory used here, including a derivation of equation (3.3), are given in Appendix II.

3.4   UPDRAFT VELOCITY

In the French-Krajewski model, calculation of the updraft velocity, w_o, is based on a model of updraft velocity originating from Georgakakos and Bras (1984). This assumes that updraft velocity varies in a piecewise linear fashion, increasing with height above the cloud base, reaching a maximum, then decreasing up to the cloud top where it attains its original value. The piecewise function is such that the vertically averaged updraft velocity, w_o, occurs at a

pressure level p_{w_o} given by

$$p_{w_o} = \tfrac{3}{4} p(z_b) + \tfrac{1}{4} p(z_t) \tag{3.4}$$

where $p(z_b)$ and $p(z_t)$ are the pressure levels at the cloud base and top respectively. If T_m is the cloud temperature at this pressure level, assuming pseudoadiabatic ascent, and T_{w_o} is the corresponding ambient air temperature, then based on an empirical relation of Sulakvelidze (1969) w_o is obtained as

$$w_o(t) = \epsilon_o \left[C_p (T_m - T_{w_o}) \right]^{1/2} \tag{3.5}$$

where ϵ_o is a parameter to be estimated. The temperatures T_m and T_{w_o} are given by parcel theory as

$$T_m = \theta_e \left[\frac{p_{w_o}}{p_n} \right]^\kappa \exp \left[\frac{-L(T_m) r_s(T_m, p_{w_o})}{c_p T_m} \right] \tag{3.6}$$

and

$$T_{w_o} = T_o \left[\frac{p_{w_o}}{p_o} \right]^\kappa . \tag{3.7}$$

3.5   RAIN WATER CONTENT OF THE CLOUD BASE

The final unknown in the mass balance equation (2.5) is M_b, the rainwater content of the cloud base. Seo and Smith estimate $M(z_b)$ by curve fitting to their known values of $M(z)$ and V_t, and using the relationship to estimate M at the cloud base z_b which is taken to be 2.5 km

7

to avoid ground clutter. They define H to be the echo-top height above z_b, and assume it to remain constant over the forecast lead time. For simplicity a linear relationship is assumed between V_L and $M_b H$ of the form

$$M_b = \frac{1}{H}\left[a(t)\,V_L(t) + b(t)\right] . \tag{3.8}$$

However, their scatter plots suggest that a power law relation might be more appropriate. By contrast, in the French-Krajewski model the value of M at the cloud base is known because z_b is taken to be the lowest level with non-zero radar reflectivity and H is the height difference between this and the highest non-zero reflectivity beam elevation. Instead, radar derived values for M, H and V_L are used to estimate by regression the parameters a and b in equation (3.8) at each time step, which are then substituted back in place of M. The calculation of M and V_L from multi-scan weather radar data is outlined in Appendix III.

3.6   SUMMARY OF DYNAMIC MODEL

Substituting the rest of the parameterised quantities (3.1), (3.2), (3.5) and (3.8) into (2.5) yields the following ordinary differential equation for the time evolution of the liquid water content in a cloud column:

$$\frac{dV_L^*}{dt} = AV_L^* + B(V_L^*)^{1+\gamma} + S \tag{3.9}$$

where the transformed variable

$$V_L^* = M_b H = a(t)\,V_L + b(t) \tag{3.10}$$

and

$$A(t) = \frac{a(t)\,w_o(t)}{H(t)} \tag{3.11}$$

$$B(t) = \frac{-a(t)}{H^{1+\gamma}}(\pi\rho_o N_o)^{-\gamma}\,\frac{\alpha}{6}\Gamma(4+\beta) \tag{3.12}$$

$$\tag{3.13}$$

$$S(t) = a(t)\,w_o(t)\left(Q_b - Q_i\right) .$$

This nonlinear ODE may be simplified and solved analytically, or integrated numerically to generate the liquid water content at the next time step. French and Krajewski choose to solve the ODE analytically via the Gauss-Taylor linearisation technique (Georgakakos & Bras, 1982) which permits the use of a Kalman Filter for real-time state-updating using radar observations. In the present study two other approaches are considered. First, a naive linearisation of the nonlinear ODE is carried out, which permits calculation of an 'exact' solution for $V_L(t)$ in each cloud column. Secondly, a fourth-order adaptive step Runge-Kutta numerical integration scheme (Press et al., 1989) is implemented yielding a solution to the full nonlinear ODE. A more detailed description of these methods is given in the next section.

To summarise, the rainfall forecasting model combines an advection scheme with a water mass balance equation and takes as input radar data, satellite observations and ground climate

data. The formulation requires estimation of two parameters, ϵ_0 in the updraft velocity equation (3.5) and $\wedge$ in the drop size distribution (modified later to $\wedge_0$ in Section 4.3). All other quantities are estimated from the available observational data.

4. Model Modifications

4.1 INTRODUCTION

This section outlines modifications that have been made to the original French-Krajewski model. The first set concern alternative methods used to solve the dynamic model equation for the time development of the vertically integrated water content in each cloud column. Other changes concern the model formulation, the mode of forecast construction, the model code configuration, accommodation of UK data, and new performance assessment measures.

4.2 ALTERNATIVE MODEL SOLUTION SCHEMES

4.2.1 Introduction

The model dynamical equation (3.9) is of the general form

$$\frac{dY}{dt} = AY + BY^{1+\gamma} + S \tag{4.1}$$

where Y(t) is the dependent variable, A, B and S can be considered constants, and $\gamma = \beta/4 = 0.1675$. In the original French-Krajewski model this is solved by statistical linearisation. Two alternative solution schemes are considered here, the first based on a "naive" linearisation and the second based on a numerical solution of the full nonlinear equation.

4.2.2 'Naive' linearisation

An approximate solution may be constructed by setting $\gamma = 0$, turning (4.1) into a linear ODE:

$$\frac{dY}{dt} = (A + B)Y + S . \tag{4.2}$$

This has the solution

$$\ln[(A + B)Y + S] = (T + k)(A + B) \tag{4.3}$$

where k is the constant of integration.

Assuming an initial condition $Y = Y_o$ when $T = T_o$, the full solution may be written

$$Y(T) = \frac{e^{\Delta T(A + B)}[(A + B)Y_o + S] - S}{(A + B)} \tag{4.4}$$

where $\Delta T = T - T_o$.

4.2.3 Numerical solution of full nonlinear equation

In this approach implementation of the full nonlinear ODE (4.1) is carried out using an adaptive step-size fifth order Runge-Kutta algorithm (Press *et al.*, 1989). This algorithm monitors local truncation error to permit adaptive stepsize control and to ensure accuracy.

4.3 OTHER MODIFICATIONS

The following changes have been made to the original French-Krajewski rainfall forecasting program:

(i)   In the original French-Krajewski model the raindrop size distribution parameter, Λ, was held constant. Following Marshall and Palmer (1948), Λ is now related to rainfall rate R (mm h^{-1}) according to

$$\Lambda = \Lambda_o R^{-0.21}$$

where Λ_o is regarded as a parameter to be estimated; a typical value of Λ_o is 4.1.

(ii)   An option within the forecasting model permits selection of one of the following methods for calculating cloud column liquid water content at the next lead time or time step. The options exhibit increasing complexity, a scheme designed to examine the behaviour of each model component in turn. Choices are as follows:

(a) **Adapted persistence**: This variant is similar to persistence in that clouds are not subject to advection or convection, rainfall being simply converted to liquid water content and back again.

(b) **Adapted advection**: In this variant clouds are converted to liquid water content, translated horizontally using an advection scheme and then converted back to rain.

(c) **Full mass-balance model**: This variant provides for the following three options:

-     French-Krajewski model formulation incorporating statistical linearisation;
-     'Naive' linearisation (assumes $\gamma = 0$); and
-     Full nonlinear ODE solved using adaptive stepsize Runge-Kutta scheme.

(iii)   The equation which finds the height of the radar beam at any point above sea-level has been replaced by one which can also take the earth's curvature into account. The new equation , based on the "four-thirds earth approximation", gives the height of the beam above Ordnance Datum as

$$h = h_0 + r \left[\frac{3}{8} \frac{r}{R} \cos\theta + \sin\theta \right]$$

where r is the range from the radar, θ is the radar beam elevation in degrees, R is the radius of the earth, and h_0 is the height of the radar above Ordnance Datum.

(iv)   A condition has been introduced that ensures that forecasts are not generated when radar data for fewer than two lowest elevation scans are present. This is necessary

because of the reduced number of radar elevation scans available in the UK data compared with weather radar data from the USA.

(v)   Disconnection of updating procedures and Kalman filtering. The model now produces state-initialised forecasts which make full use of all available data at each forecast time origin.

(vi)   Reorganisation of the forecasting component of model to allow any number of forecasts, at user-specified lead times.

(vii)   The following performance measures are calculated to assess model performance:

Mean Error
Root Mean Square Error (rmse)
Root Mean Square Log Error (rmsle)
R^2 goodness of fit
Critical Success Index (CSI)
False Alarm Rate (FAR)
Probability of Detection (POD)

The first five are used in practice. Further details of these performance measures are given in Appendix IV.

5. Incorporation of data into forecasting model

5.1 INTRODUCTION

This section outlines the observation data needed to run the rainfall forecast model along with data helpful in the interpretation of results and in the development of new model parameterisations. Any preprocessing of the raw data needed prior to use in the model is discussed. The model requires data from a multi-scanning weather radar, surface climate stations, and from satellite imagery. These are considered in turn followed by mention of radiosonde and disdrometer data which, whilst not currently used directly in the model, are thought of value to the study. Examples of some of these data are given for the severe storms occurring over southern Britain during the period 8 to 12 June 1993 which have been used in initial trials of the model.

5.2 WEATHER RADAR DATA

The original model of French and Krajewski was developed for use with data from the WSR-74S S-band, 2.2° beamwidth radars which make up the quasi-operational RADAP II network in the USA. Volume scan data from the Oklahoma city radar were used in the form of reflectivity observations at 12 antenna elevations: 0.5° and at 2° increments from 2° to 22°. In contrast, the C-band, 1° beamwidth radars which make up the UK network routinely scan at only 4 elevations: 0.5°, 1.5°, 2.5° and 4°. This means that, within about 80 km range of the radar, sensing of the atmosphere by the radar does not extend sufficiently high to measure the potentially moistest parts of the troposphere (Figure 5.2.1).
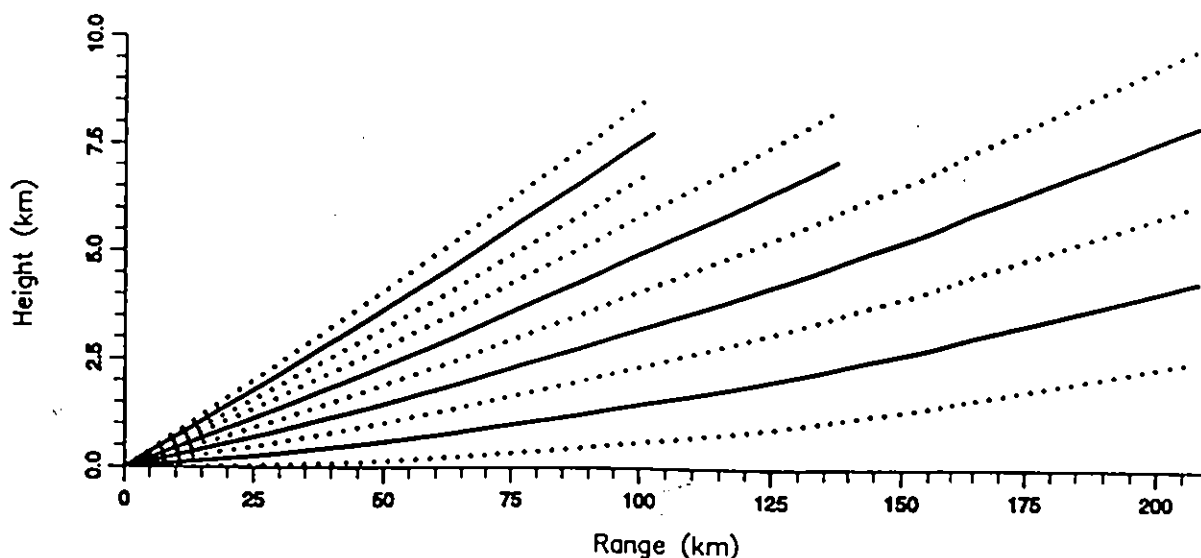

Figure 5.2.1 UK weather radar scan elevations showing beam height and width as a function of range

13

The problem presented by the paucity of elevation scans and their limited vertical extent at closer ranges to the radar has been addressed by interpolating the radar data onto a regular three-dimensional grid. An extension of the two-dimensional multiquadric surface fitting method, developed by Moore *et al.* (1988, 1991), to three dimensions has been used. Details of the method are given in Appendix V.

Only the 0.5° elevation scan data within a 76 km range of the radar are available on a Cartesian 2 km grid. Since data for all four elevation scans are available on a Cartesian 5 km 84 by 84 grid out to a range of 210 km, these have been used in the initial development of the model to UK conditions. Since these data are irregularly spaced in the vertical, the interpolation scheme is used to map these onto a regular grid. This grid has 15 points spaced 1 km apart in the vertical and 84 by 84 points spaced 5 km apart in the horizontal.

5.3   SURFACE CLIMATE STATION DATA

The model requires data for air temperature, dew point temperature and pressure from surface observing stations. A set of 15 stations extending over southern England and Wales has been identified to support the study (Table 5.3.1, Figure 5.3.1). Data for these synoptic stations are held in the UK Met. Office's Synoptic Data Bank for a sampling interval of one hour. For use in the model these data are interpolated onto the same 84 by 84, 5 km grid as the radar data using the two-dimensional multiquadric surface fitting technique. The scaling length in the exponential distance function of the interpolation scheme is increased from 20 to 200 km to reflect the larger spacing of the synoptic stations. Examples of the interpolated fields are shown in Figure 5.3.2. In the future data from the HYREX Automatic Weather Station (AWS) in the Brue catchment, installed on 2 September 1993, will be employed in the model. This AWS provides air temperature, wet bulb temperature and pressure data at a 15 minute sampling interval.

5.4   SATELLITE DATA

The model requires cloud top temperature data derived from satellite imagery. A primary receiving station, operating at the Institute of Hydrology, Wallingford, has routinely captured Meteosat data over the UK for a 30 minute sampling interval since 21 August 1993. Prior to this data are available from the Met. Office archive for a 60 minute sampling interval. For use in the model the satellite cloud top temperature data are interpolated onto the same 84 by 84, 5 km grid as the radar data. Again the two-dimensional multiquadric interpolation scheme is used. Only satellite data for points lying within 15 km of a 5 km pixel are used in the interpolation. Examples of regular grid brightness temperature fields are shown in Figure 5.4.1.

5.5   RADIOSONDE DATA

Whilst radiosonde data are not required in the current form of the model, such data should prove useful to support interpretation of the results and in developing new model parameterisations. Six radiosonde stations in southern England and Wales have been identified as useful to the model study. These are summarised in Table 5.5.1. They provide data on height, pressure, temperature, dew-point temperature, wind speed and wind direction. The frequency of radiosonde launching is variable, being as frequent as 6-hourly at Herstmonceux

Table 5.3.1 *Synoptic observing stations in southern England and Wales*

Station name	Station number	National Grid Reference
Bedford R.A.E.	3558	5038 2591
Wyton	3566	5280 2741
Wattisham	3590	6033 2511
Cilfynydd	3614	3100 1932
Benson SAWS	3657	4623 1917
Benson	3658	4637 1917
Stansted Airport	3683	5535 2226
Shoeburyness	3693	5962 1873
Walton-on-Naze	3696	6259 2220
Lundy	3702	2148 1446
Cardiff-Wales Airport	3715	3061 1677
Netheravon	3745	4161 1502
Culdrose	3809	1675 0251
Yeovilton	3853	3558 1225
Portland/RNAS	3858	3681 0746

1 (3558)
2 (3566)
3 (3590)
4 (3614)
5 (3657)
6 (3658)
7 (3683)
8 (3693)
9 (3696)
10 (3702)
11 (3715)
12 (3745)
13 (3809)
14 (3853)
15 (3858)
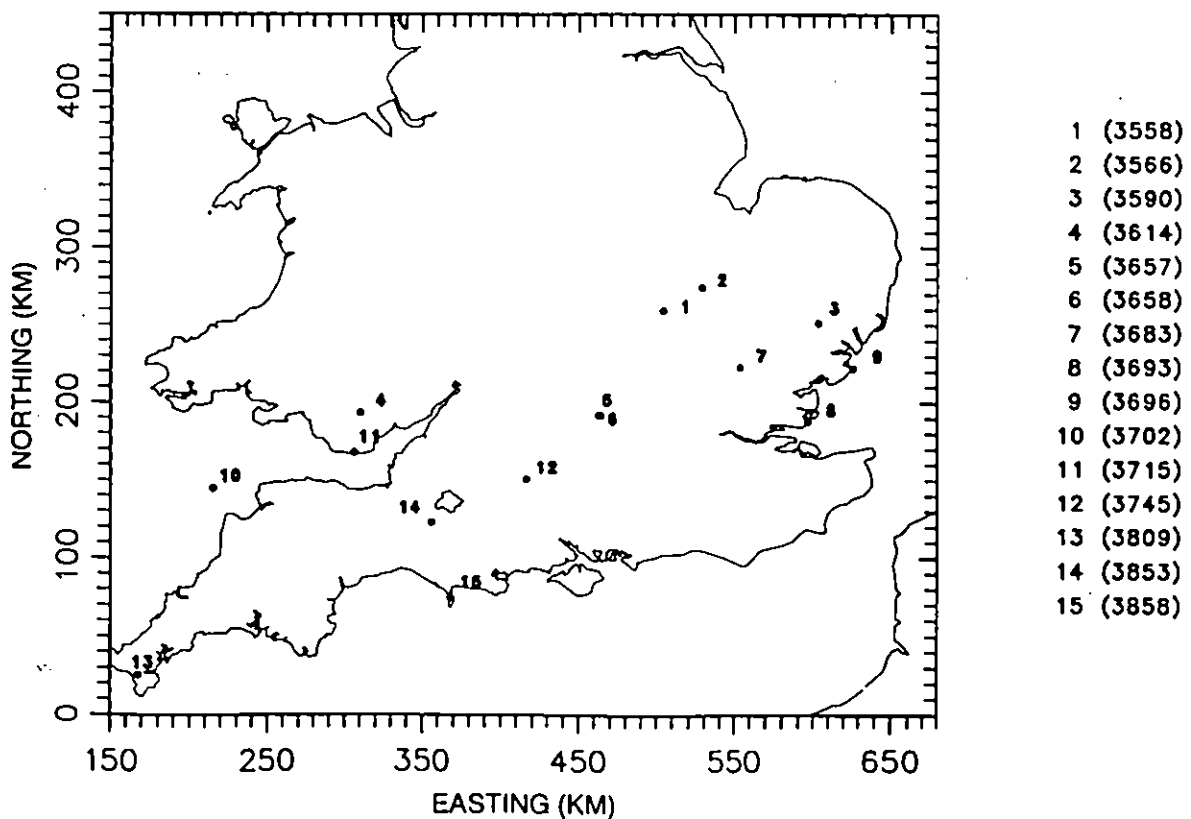
Figure 5.3.1 *Locations of synoptic stations in southern England and Wales.*

(a)   *Pressure (mb)*

ABOVE	1010.8
1010.1 –	1010.8
1009.5 –	1010.1
1008.8 –	1009.5
1008.1 –	1008.8
1007.5 –	1008.1
1006.8 –	1007.5
1006.2 –	1006.8
1005.5 –	1006.2
1004.8 –	1005.5
1004.2 –	1004.8
1003.5 –	1004.2
1002.8 –	1003.5
1002.2 –	1002.8
1001.5 –	1002.2
1000.9 –	1001.5
1000.2 –	1000.9
BELOW	1000.2

(b)   *Temperature (°K)*

ABOVE	289.1
288.8 –	289.1
288.5 –	288.8
288.2 –	288.5
287.9 –	288.2
287.6 –	287.9
287.3 –	287.6
287.0 –	287.3
286.7 –	287.0
286.4 –	286.7
286.1 –	286.4
285.8 –	286.1
285.5 –	285.8
285.2 –	285.5
284.9 –	285.2
284.6 –	284.9
284.3 –	284.6
BELOW	284.3

Figure 5.3.2 *Interpolated fields using synoptic climate station data for 20:00 11 June 1993*

16

(c)   *Dew point temperature (°K)*
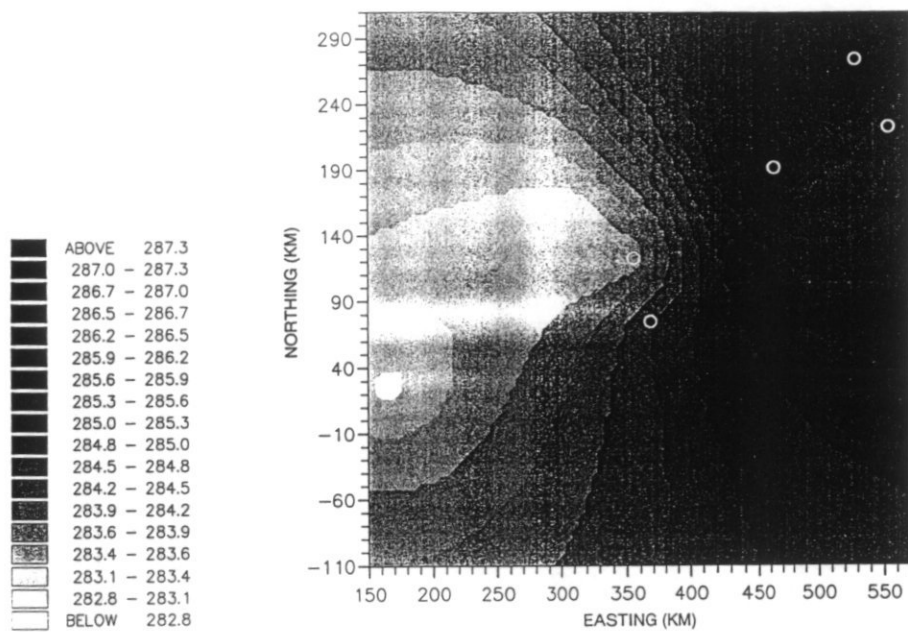
(d)   *Wet bulb depression (°K)*
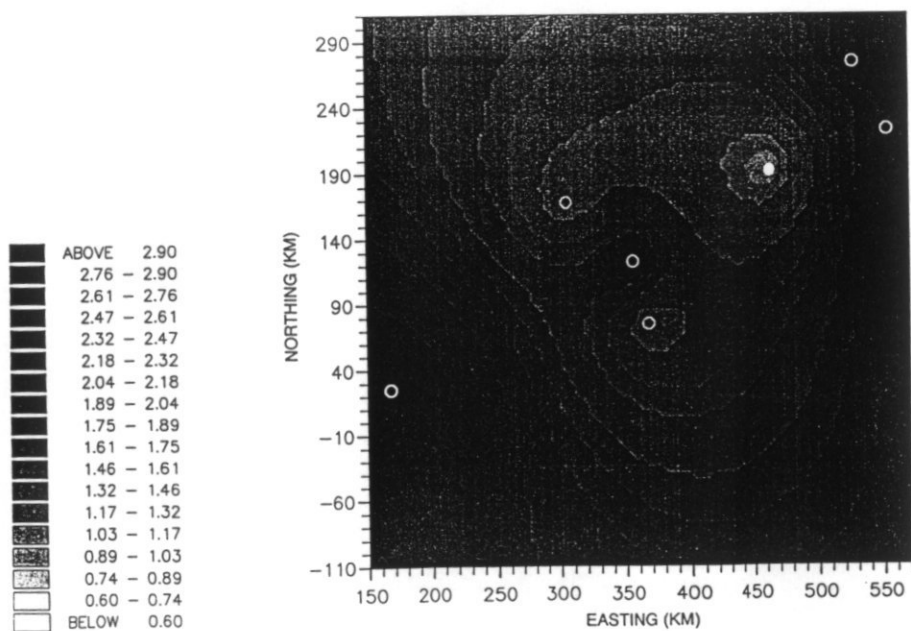
Figure 5.3.2 *(continued) Interpolated fields using synoptic climate station data for 20:00 11 June 1993*

17

(a)   *18:00 9 June 1993*
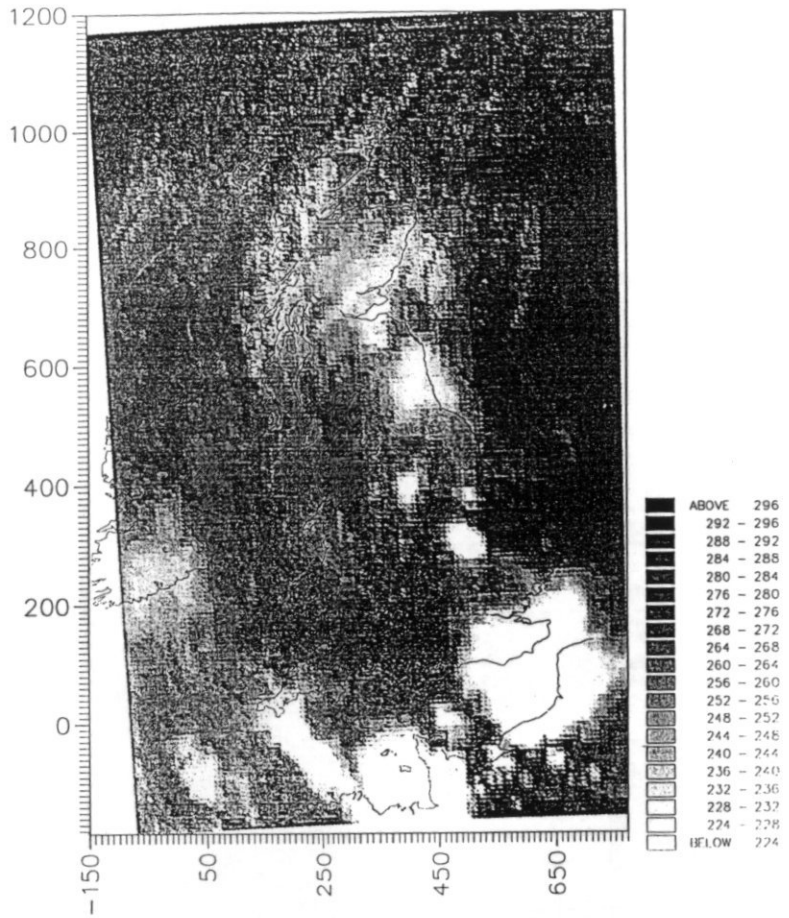
(b)   *20:00 11 June 1993*
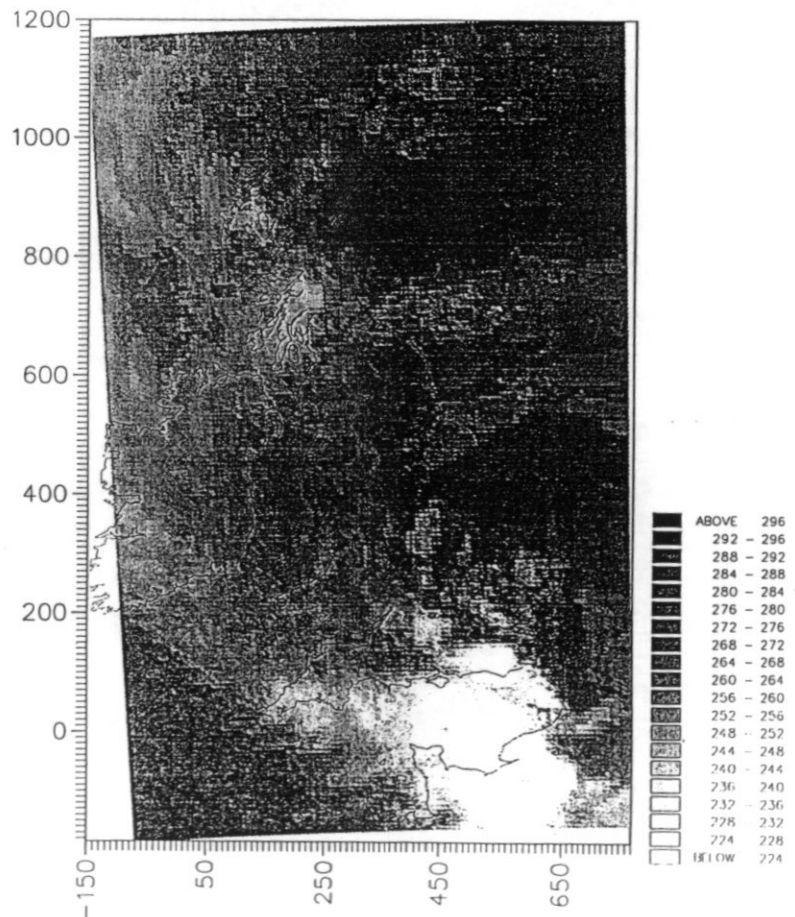
Figure 5.4.1 *Examples of satellite brightness temperature fields over the UK*

18

but, for example, varying from 7 to .18 hours at Larkhill and from 11 to 13 hours at Camborne. Data are held in the Met. Office Synoptic Data Bank.

As part of a special HYREX Intense Observing Period programme radiosondes will be launched for selected storms from the Brue AWS site by researchers at the Joint Centre for Mesoscale Meteorology, University of Reading. At the same time the Institute of Hydrology will operate a disdrometer at this site to support studies aimed at parameterising drop size distributions for improved radar estimation of cloud water content and rain rate in the model.

6. Assessment of rainfall forecasting model

6.1 INTRODUCTION

An initial assessment of the current form of the rainfall forecasting model has been undertaken using data for the period 8 to 12 June 1993 when a number of thunderstorms occurred over southern Britain . The geographic area for assessment is the area scanned by the Wardon Hill radar in Dorset. This is located about 40 km from the Brue catchment which forms the focus of the HYREX study area (Figure 6.1.1).

A description of the events used for evaluation are given next. This is followed by a detailed analysis of model performance at different lead times, and in particular, for a one hour lead time.
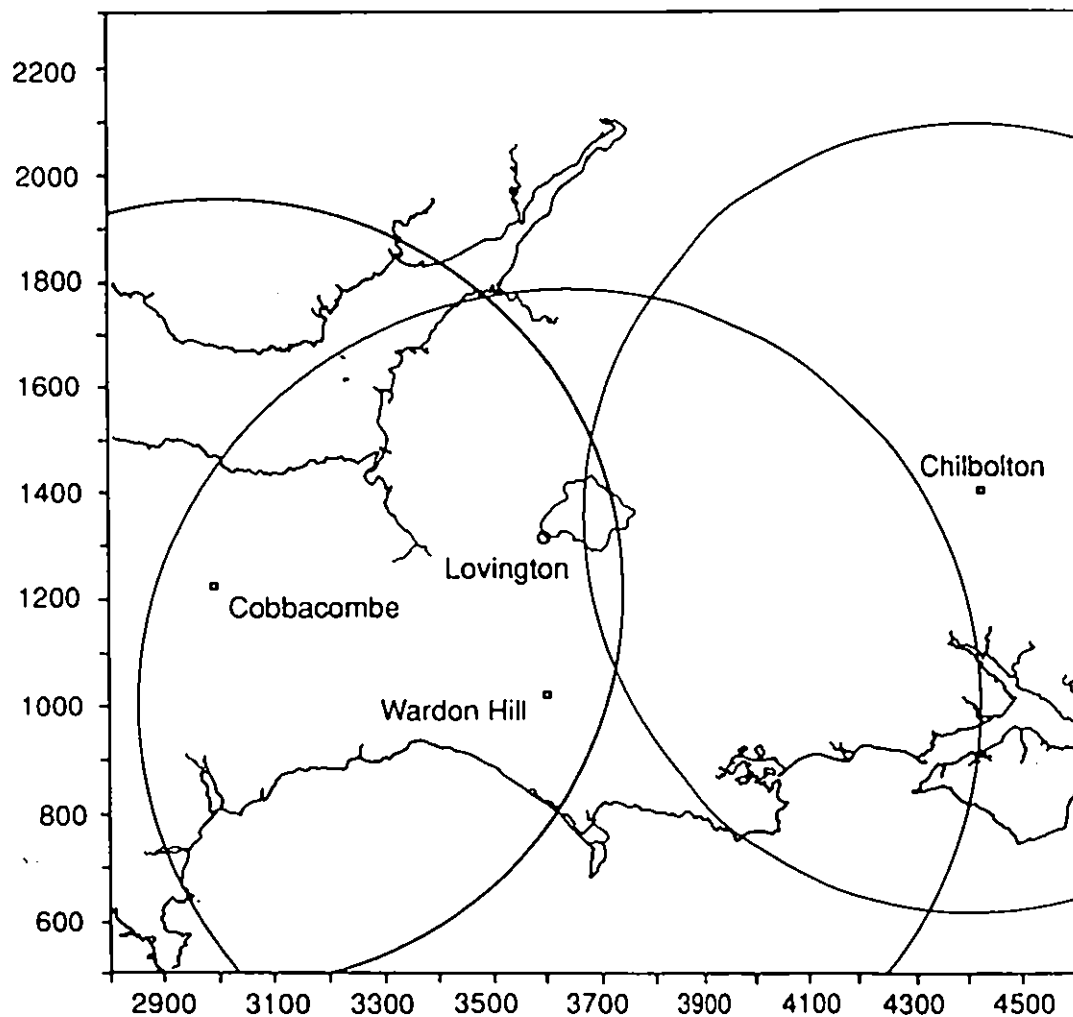
Figure 6.1.1 The Wardon Hill radar within the HYREX study area.

8 June 1993
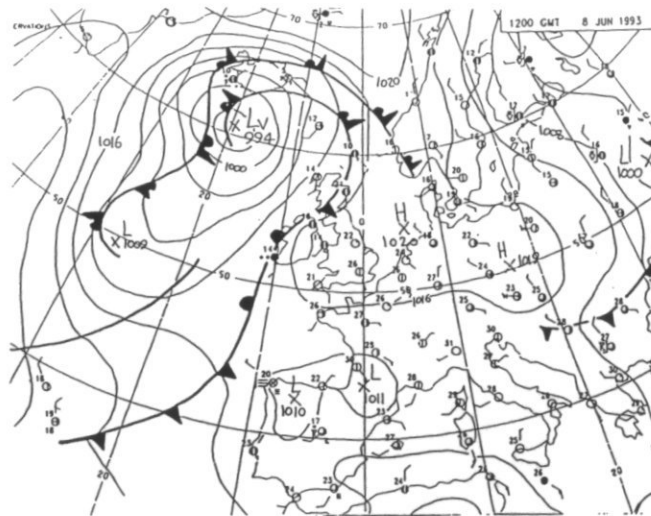
9 June 1993
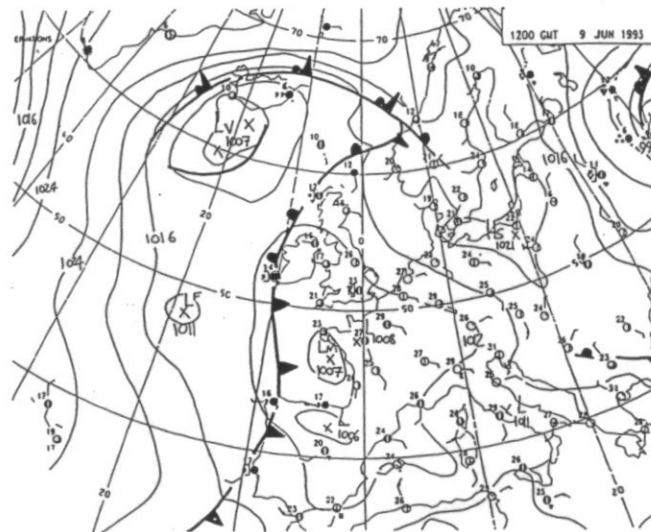
10 June 1993
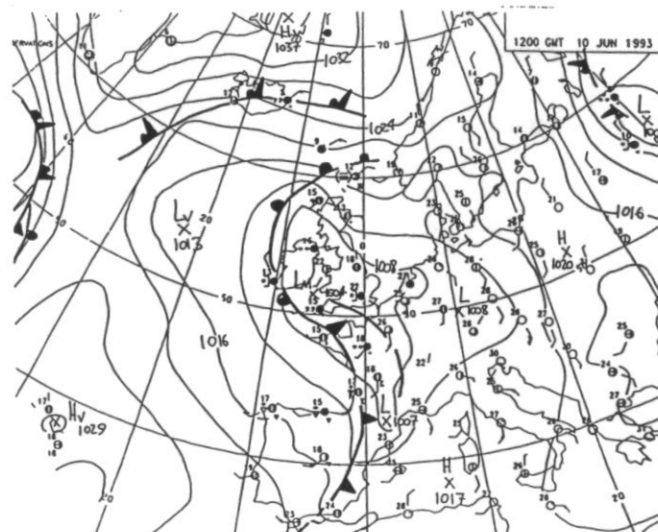
Figure 6.2.1 *Midday synoptic charts for the assessment period*

22

6.2 DESCRIPTION OF RAINFALL EVENTS

The following provides a summary of the weather situation for the period 8 to 12 June 1993 used in the assessment. Descriptions and midday weather charts have been gleaned from the Met. Office Daily Weather Summaries, the Journal of Meteorology and Weather magazine.

8 June 1993: High pressure prevailed over much of England, although by midnight, low pressure in the south was pushing northwards. The maximum temperature in the southwest was about 25°C and the air was very humid.

**9 June 1993:** The anticyclone receded to the Baltic to be replaced by low pressure. A thunderstorm arrived off the Cornish coast late on the 8th and Cornwall experienced a severe thunderstorm during the night. Throughout the morning thunderstorms broke out elsewhere too. The middle part of the day was drier and clearer, but in the evening, as the low centre moved over England, the cold front edged into southern England and there were more thunderstorms and rain. The day was very warm and muggy, with light winds.

10 June 1993: The low was centred over the country, with a cold front prevailing. It was warm and humid, with light winds. A thundery airmass encompassed most of the country and thunderstorms were widespread. They were concentrated along the cold frontal zone from North Wales, through the Midlands, to London. An isolated thunderstorm occurred, in, and around Barnstaple, in Devon. In the southwest, rainfall was generally lighter.

11 June 1993: There was a deepening depression centred over Wales. Much colder air encroached into Devon, Cornwall and South Wales. Storms and prolonged, widespread, heavy rain brought extensive flooding to large areas of Wales and the West Country. It was cool in the southwest, with maximum temperatures less than 15°C and very windy.

12 June 1993: Frontal conditions weakened. Rain was widespread and heavy in southwest England and Wales overnight. Much of England and Wales had a cloudy, cool day. Southwest England had further heavy rain in the morning. In the afternoon, there were isolated thunderstorms in the south.

Midday charts for the above 5 days are shown in Figure 6.2.1

6.3 ASSESSMENT OF MODEL PERFORMANCE

From the 5 days of available data, a set of six events, each extending over an eight hour period, were chosen for model assessment. Other possible events had been discarded, usually because of missing data or insufficient rain. The six events are listed in Table 6.3.1 along with an indication of the predominant storm type for each event. Note that events 1 and 2 are predominantly convective, 3, 4 and 5 are frontal and 6 is of mixed type. The possible presence of solid precipitation in each event, which might adversely affect the model results, is investigated in Appendix VI. It is concluded that the frontal events 3, 4 and 5 may be affected by solid precipitation, particularly event 5, later on in the day. There is no firm evidence that the convective events are affected.

At each timestep (time origin) in an event, state initialised forecasts, along with the set of performance statistics (Appendix IV), were calculated for the four lead times 15, 30, 45 and

21

Table 6.3.1 Eight hour duration events used for model assessment

Event	Start	End	Predominant Storm type
1	23:57 9/6/93	07:57 10/6/93	Convective
2	15:57 10/6/93	23:57 10/6/93	Convective
3	00:57 11/6/93	08:57 11/6/93	Frontal
4	08:57 11/6/93	16:57 11/6/93	Frontal
5	16:57 11/6/93	00:57 12/6/93	Frontal
6	08:57 12/6/93	16:57 12/6/93	Mixed

Table 6.3.2 Assessment of different model variants (a) rmse statistic

Event number	Start of event	Model variant	Lead Time (mins) 15	30	45	60
1	23:57 9/6/93	P	3.904	3.815	3.848	3.915
		A	6.391	7.021	6.664	6.799
		D-SL	5.321	5.362	4.681	4.433
		D-L	5.189	5.102	4.395	4.124
		D-NL	4.733	4.421	3.740	3.584
2	15:57 10/6/93	P	9.169	9.462	9.439	9.420
		A	8.401	9.336	9.509	9.335
		D-SL	7.584	7.777	7.381	6.821
		D-L	7.279	7.273	6.758	6.122
		D-NL	5.998	5.538	4.986	4.450
3	00:57 11/6/93	P	2.720	2.794	2.852	2.893
		A	3.016	3.446	3.712	3.875
		D-SL	2.765	2.985	3.106	3.176
		D-L	2.609	2.725	2.752	2.741
		D-NL	2.111	2.075	2.079	2.100
4	08:57 11/6/93	P	2.811	2.952	3.047	3.125
		A	2.618	2.997	3.238	3.405
		D-SL	2.475	2.694	2.813	2.883
		D-L	2.343	2.470	2.513	2.521
		D-NL	1.961	1.953	1.974	2.002
5	16:57 11/6/93	P	1.277	1.341	1.385	1.416
		A	1.041	1.239	1.344	1.406
		D-SL	1.096	1.252	1.347	1.407
		D-L	1.090	1.235	1.315	1.358
		D-NL	1.076	1.199	1.261	1.287
6	08:57 12/6/93	P	1.687	1.746	1.783	1.814
		A	1.678	1.757	1.799	1.805
		D-SL	1.781	1.764	1.762	1.767
		D-L	1.719	1.680	1.675	1.658
		D-NL	1.530	1.499	1.523	1.533

Key:
P   Adapted persistence
A   Adapted advection
D-SL   Dynamic model - statistical linearisation
D-L   Dynamic model - linear approximation
D-NL   Dynamic model - nonlinear

11 June 1993
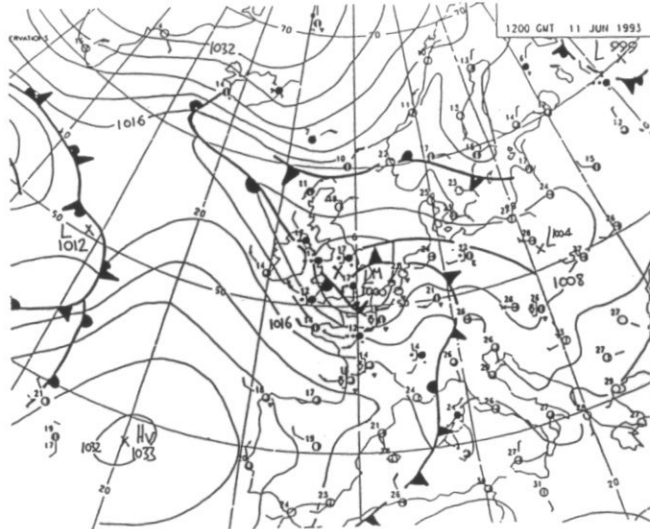
12 June 1993
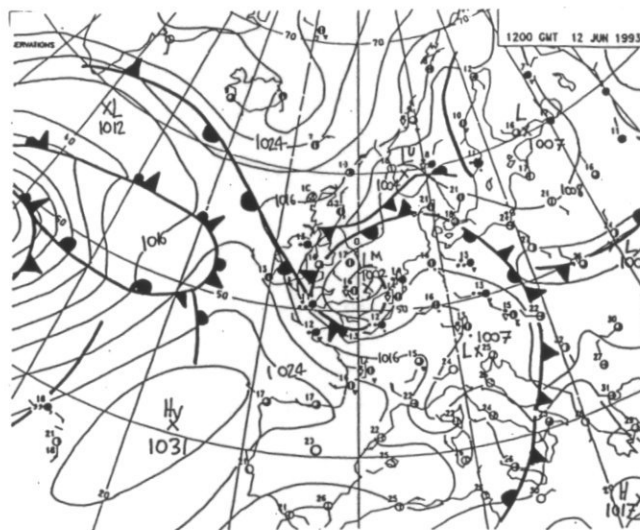
Figure 6.2.1 *cont. Midday synoptic charts for the assessment period*

Table 6.3.2 cont.   Assessment of different model variants (b) rmsle statistic

Event number	Start of event	Model	Lead Time (mins)			
			15	30	45	60
1	23:57 9/6/93	P	0.823	0.813	0.813	0.829
		A	0.630	0.712	0.703	0.742
		D-SL	0.785	0.839	0.821	0.855
		D-L	0.778	0.824	0.803	0.831
		D-NL	0.768	0.801	0.773	0.794
2	15:57 10/6/93	P	0.898	0.942	0.965	0.982
		A	0.482	0.632	0.716	0.770
		D-SL	0.575	0.696	0.770	0.822
		D-L	0.570	0.683	0.750	0.798
		D-NL	0.555	0.654	0.710	0.750
3	00:57 11/6/93	P	0.785	0.809	0.827	0.841
		A	0.421	0.559	0.640	0.697
		D-SL	0.414	0.544	0.624	0.683
		D-L	0.406	0.525	0.596	0.646
		D-NL	0.387	0.492	0.552	0.596
4	08:57 11/6/93	P	0.647	0.688	0.716	0.739
		A	0.420	0.533	0.603	0.652
		D-SL	0.432	0.534	0.598	0.644
		D-L	0.426	0.519	0.576	0.615
		D-NL	0.409	0.492	0.540	0.573
5	16:57 11/6/93	P	0.4651	0.498	0.523	0.541
		A	0.361	0.444	0.495	0.530
		D-SL	0.398	0.466	0.513	0.548
		D-L	0.399	0.465	0.509	0.540
		D-NL	0.340	0.462	0.502	0.529
6	08:57 12/6/93	P	0.588	0.613	0.631	0.643
		A	0.393	0.474	0.518	0.545
		D-SL	0.502	0.556	0.591	0.617
		D-L	0.499	0.550	0.581	0.602
		D-NL	0.493	0.538	0.565	0.583

Key: P   Adapted persistence
   A   Adapted advection
       D-SL   Dynamic model - statistical linearisation
       D-L   Dynamic model - linear approximation
       D-NL   Dynamic model - nonlinear

Table 6.3.2 cont. Assessment of different model variants (c) CSI statistic

Event number	Start of event	Model	Lead Time (mins)			
			15	30	45	60
1	23:57 9/6/93	P	0.087	0.068	0.070	0.072
		A	0.350	0.271	0.272	0.243
		D-SL	0.285	0.212	0.225	0.190
		D-L	0.285	0.212	0.225	0.190
		D-NL	0.284	0.211	0.224	0.189
2	15:57 10/6/93	P	0.423	0.381	0.341	0.312
		A	0.457	0.411	0.368	0.331
		D-SL	0.413	0.368	0.323	0.282
		D-L	0.413	0.368	0.322	0.282
		D-NL	0.413	0.368	0.321	0.281
3	00:57 11/6/93	P	0.346	0.332	0.317	0.303
		A	0.615	0.582	0.550	0.523
		D-SL	0.612	0.580	0.548	0.521
		D-L	0.612	0.580	0.548	0.521
		D-NL	0.612	0.580	0.548	0.521
4	08:57 11/6/93	P	0.714	0.698	0.680	0.664
		A	0.760	0.734	0.713	0.697
		D-SL	0.752	0.727	0.708	0.694
		D-L	0.752	0.726	0.706	0.692
		D-NL	0.752	0.725	0.706	0.692
5	16:57 11/6/93	P	0.731	0.708	0.687	0.668
		A	0.755	0.725	0.704	0.687
		D-SL	0.733	0.700	0.678	0.659
		D-L	0.733	0.698	0.674	0.653
		D-NL	0.735	0.698	0.673	0.651
6	08:57 12/6/93	P	0.328	0.278	0.240	0.211
		A	0.498	0.435	0.389	0.351
		D-SL	0.370	0.328	0.293	0.262
		D-L	0.370	0.328	0.293	0.261
		D-NL	0.371	0.328	0.293	0.262

Key:
P   Adapted persistence
A   Adapted advection
D-SL   Dynamic model - statistical linearisation
D-L   Dynamic model - linear approximation
D-NL   Dynamic model - nonlinear

60 minutes. For this initial assessment the two model parameters, ϵ_0 and Λ_0, have been set at values of 0.002 and 8 respectively. Table 6.3.2 summarises the results obtained for each model variant in terms of the rmse, rmsle and CSI performance measures.

The tables indicate that the frontal events 3,4 and 5 were the most accurately forecast with Critical Success Index (CSI) values in the region of 0.6 to 0.7 and comparatively low rmse and rmsle values. In comparison, the convective storm events 1 and 2 are quite poorly forecast with high rmse and rmsle and low values of the CSI. The mixed event, number 6, is not as well forecast as the frontal events, but the results are not as poor as those obtained for convective storms.

Figure 6.3.1 shows the one hour ahead forecast rainfall fields for the time periods 18:22 10/6/93 and 10:12 11/6/93, providing examples of forecasts for convective and frontal conditions respectively. The observed rainfall fields are shown together with those forecast using the five different model variants. Those for the frontal event support the view that the model is able to forecast the temporal development of frontal events reasonably well. They show that the nonlinear model variant performs best at forecasting rainfall intensities whilst the adapted-persistence and advection methods, in particular, result in overestimation of intensities. The forecast fields for the convective storm example are less encouraging with overestimation in intensity leading to unrealistic rainfall estimates. This is particularly apparent in adapted-persistence and advection forecasts whilst the nonlinear model variant provides some improvement. However, overall, observed and forecast rainfall fields are quite dissimilar, with poor positioning of rainfall leading to the low values of CSI, indicating that the model is unable to forecast the development of convective storms very well. Figure 6.3.2 illustrates the difficulties involved in forecasting rapidly changing convective storms. Here, the rainfall field one hour previous to the forecast field, referred to as actual persistence, is displayed alongside the observed and forecast fields. The field observed one hour before at 1:30 is used in the forecast of the rainfall at 2:30. Since the radar measures very little rainfall in the first field, this leads to underestimation in the forecast field for all model variants.

Figures 6.3.3 show graphically how rmsle, rmse, CSI and mean error, for the one hour ahead forecast for each model variant, vary through each of the six events of eight hours duration. The results confirm those deduced from the table of results at various lead times over the whole eight hours. Again, poor CSI and high values of error are observed for convective events, whilst lower errors and higher Critical Success Index values are obtained for frontal storms. The nonlinear model variant frequently gives the best forecast fields, with the 'naive' linear dynamic model also performing well.

6.4 DISCUSSION OF RESULTS

Comparison of a 'standard' persistence forecast with that obtained via adapted-persistence (summing up estimated rainfall for each radar scan elevation to form the vertically integrated water content, V_L and then converting it back into rain via an equation relating V_L to cloud-base water content and cloud height) suggests that the latter method leads to greatly overestimated rainfall intensities, particularly in the case of convective storms. This could be due to a number of possible causes, including the following:

27

Observed

Adapted persistence

Adapted advection

Dynamic - statistical linearisation

Dynamic - linear

Dynamic - nonlinear

ABV		130.0
121.9	—	130.0
113.8	—	121.9
105.6	—	113.8
97.5	—	105.6
89.4	—	97.5
81.3	—	89.4
73.1	—	81.3
65.0	—	73.1
56.9	—	65.0
48.8	—	56.9
40.6	—	48.8
32.5	—	40.6
24.4	—	32.5
16.3	—	24.4
8.1	—	16.3
0.0	—	8.1
BLW		0.0
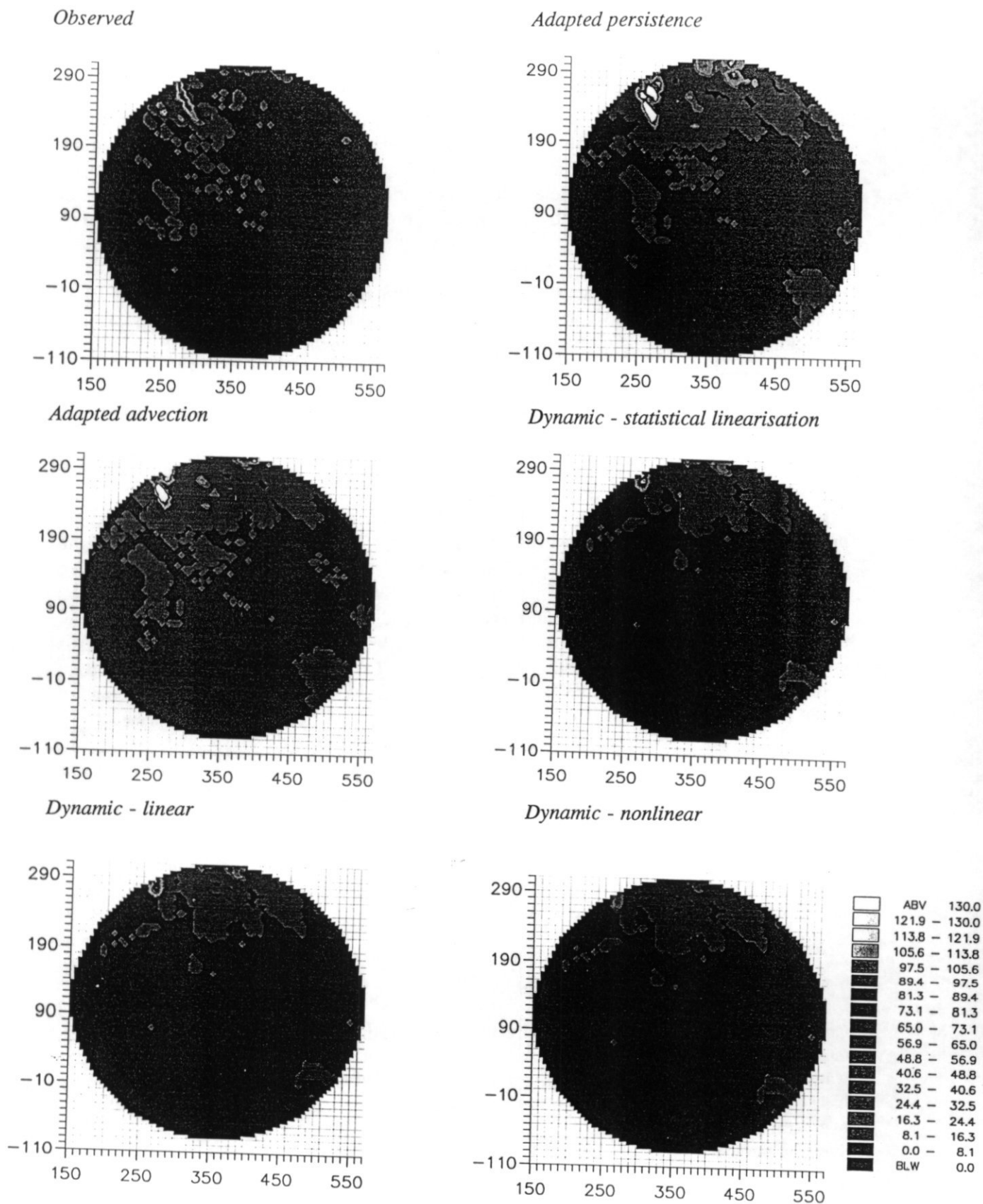
Figure 6.3.1 One hour ahead forecast rainfall fields (a) Convective event, 18:12 10/6/93.

Observed

Adapted persistence

Adapted advection

Dynamic - statistical linearisation

Dynamic - linear

Dynamic - nonlinear

|	
ABV	40.0
37.5 —	40.0
35.0 —	37.5
32.5 —	35.0
30.0 —	32.5
27.5 —	30.0
25.0 —	27.5
22.5 —	25.0
20.0 —	22.5
17.5 —	20.0
15.0 —	17.5
12.5 —	15.0
10.0 —	12.5
7.5 —	10.0
5.0 —	7.5
2.5 —	5.0
0.0 —	2.5
BLW	0.0
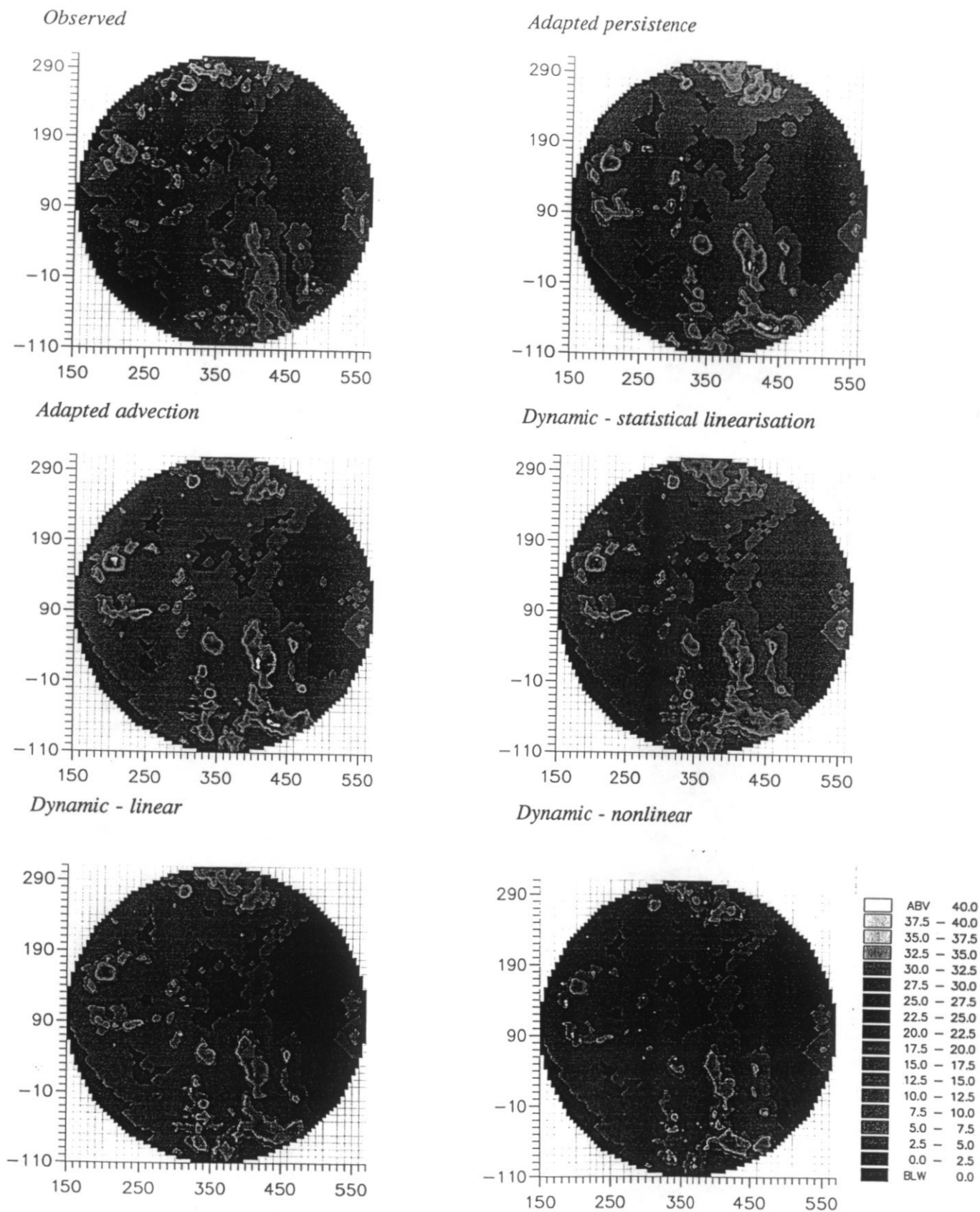
Figure 6.3.1 *cont. One hour ahead forecast rainfall fields (b) Frontal event, 10:12 11/6/93.*

29

Observed

Actual persistence
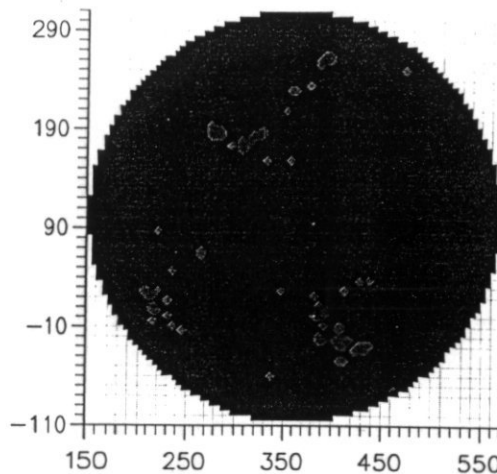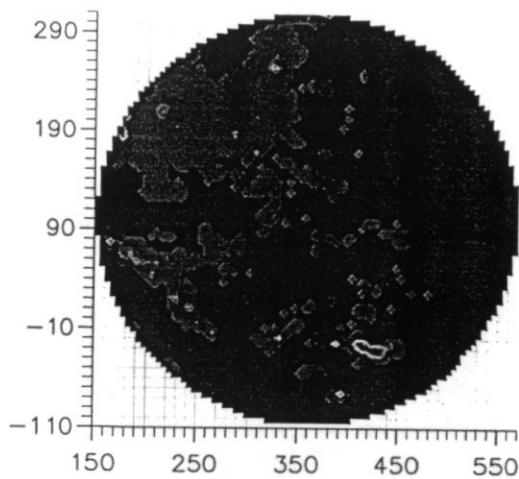
Dynamic nonlinear

Adapted persistence

	ABV	120.0
	112.5 —	120.0
	105.0 —	112.5
	97.5 —	105.0
	90.0 —	97.5
	82.5 —	90.0
	75.0 —	82.5
	67.5 —	75.0
	60.0 —	67.5
	52.5 —	60.0
	45.0 —	52.5
	37.5 —	45.0
	30.0 —	37.5
	22.5 —	30.0
	15.0 —	22.5
	7.5 —	15.0
	0.0 —	7.5
	BLW	0.0
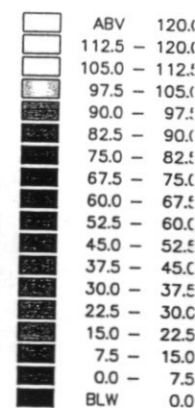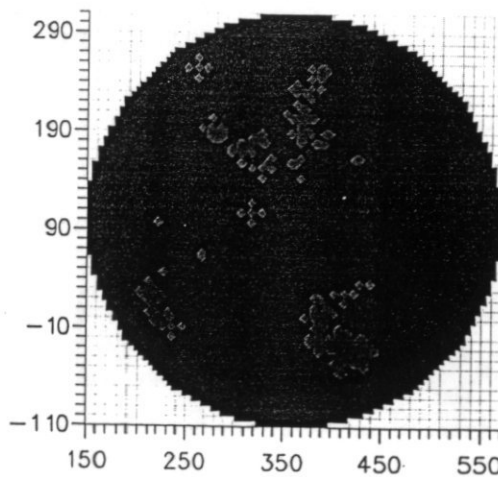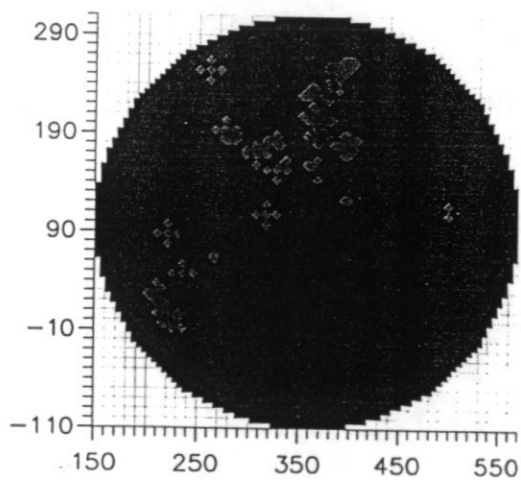
Figure 6.3.2 *Illustration of the difficulty of forecasting a rapidly changing convective field; one hour ahead forecast of observed field at 2:30 10 June 1993*
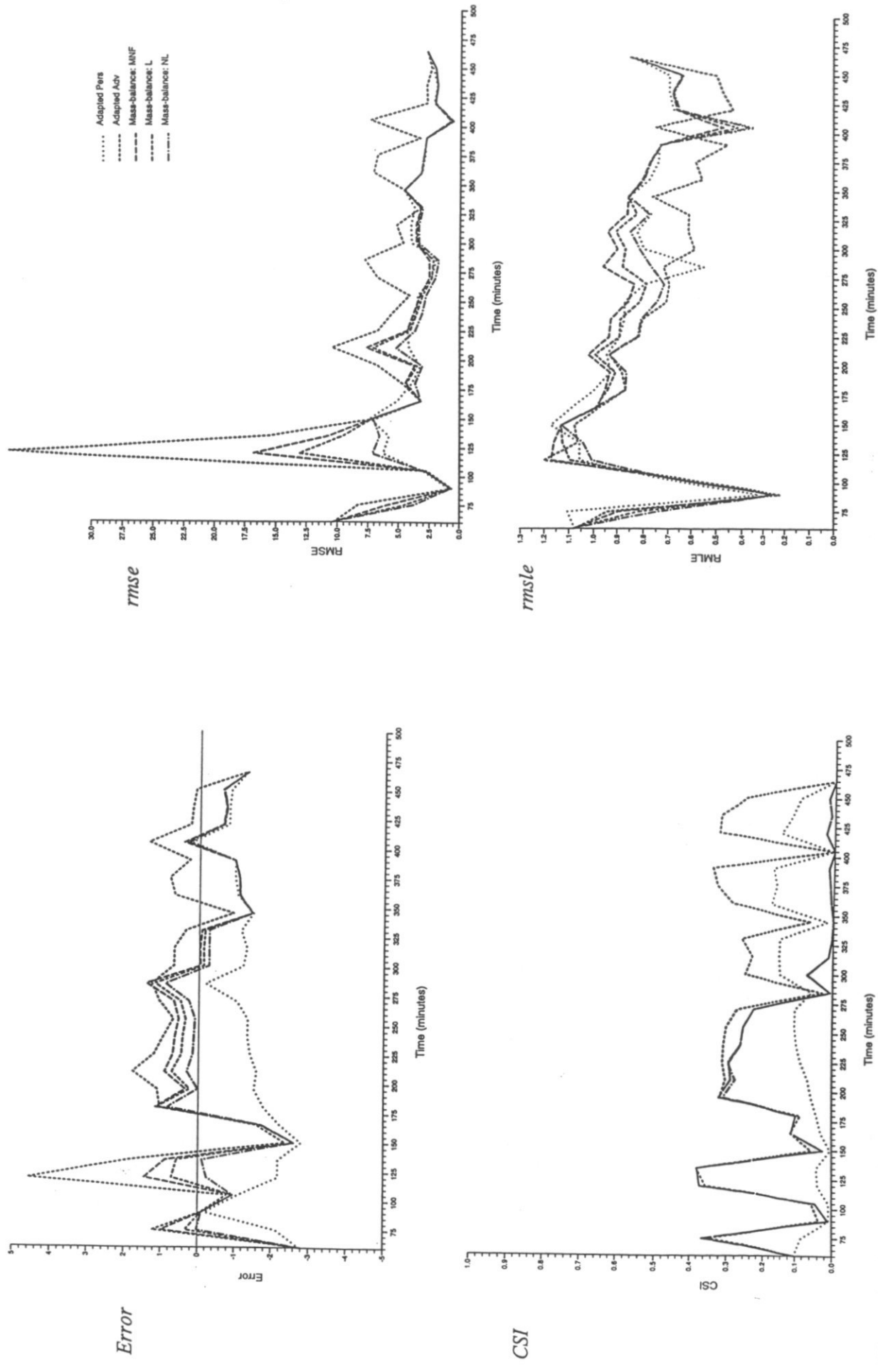
Figure 6.3.3 Evolution of the one hour ahead forecast error statistics over the eight hour duration event (a) Event 1 9 June 1993
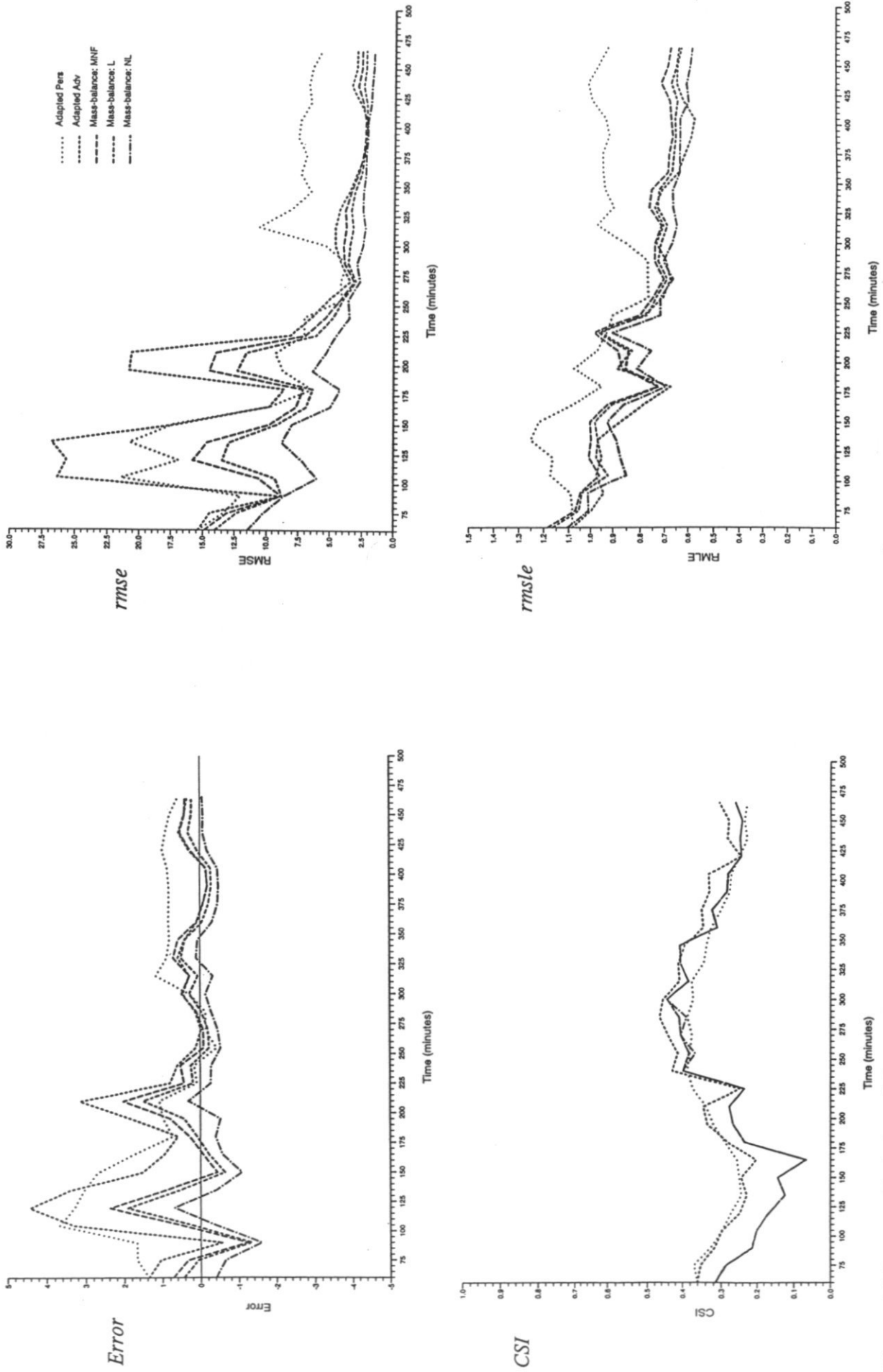
31

Figure 6.3.3 cont. Evolution of the one hour ahead forecast error statistics over the eight hour duration event (b) Event 2 10 June 1993
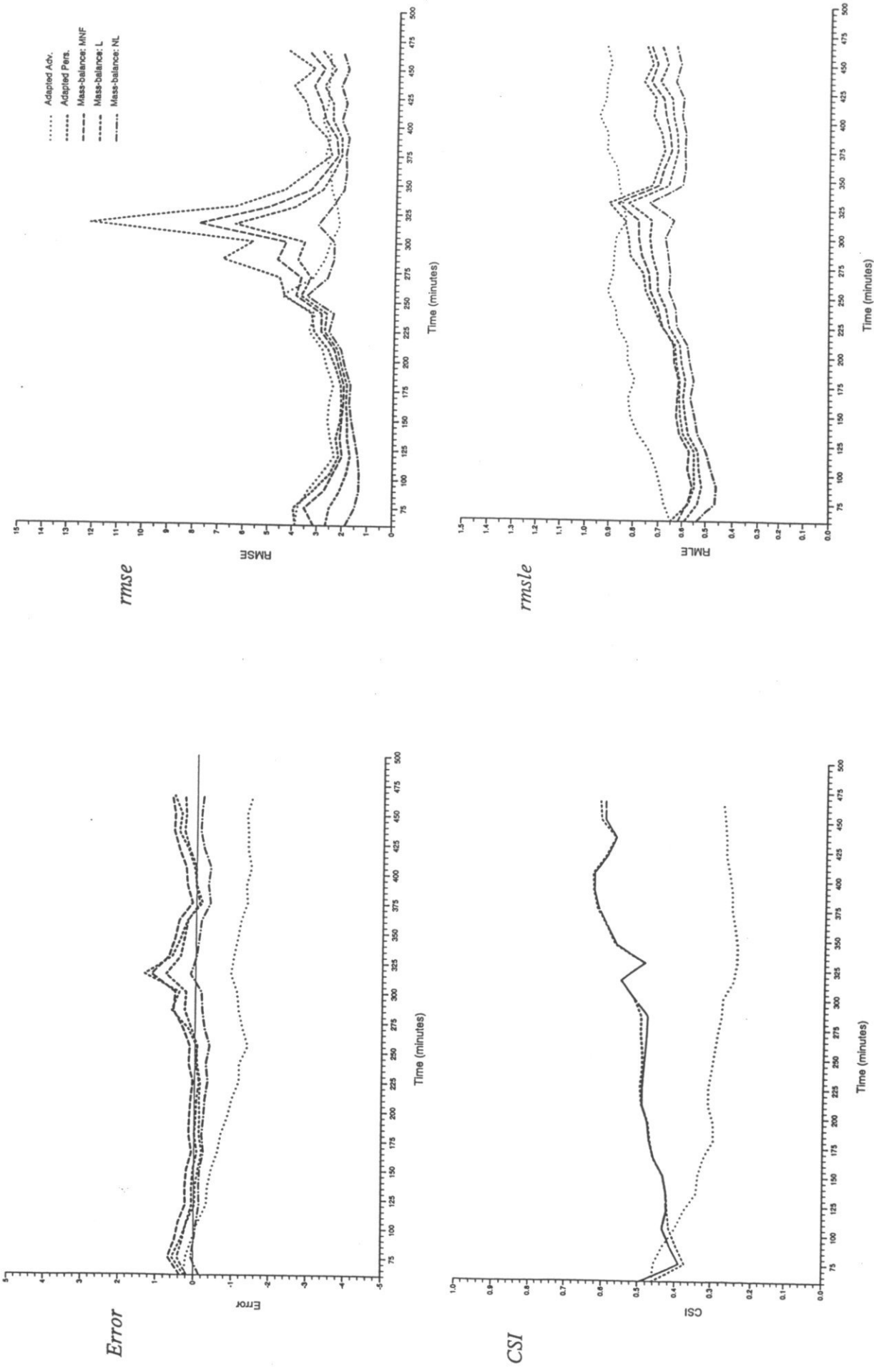
Figure 6.3.3 cont. Evolution of the one hour ahead forecast error statistics over the eight hour duration event (c) Event 3 11 June 1993
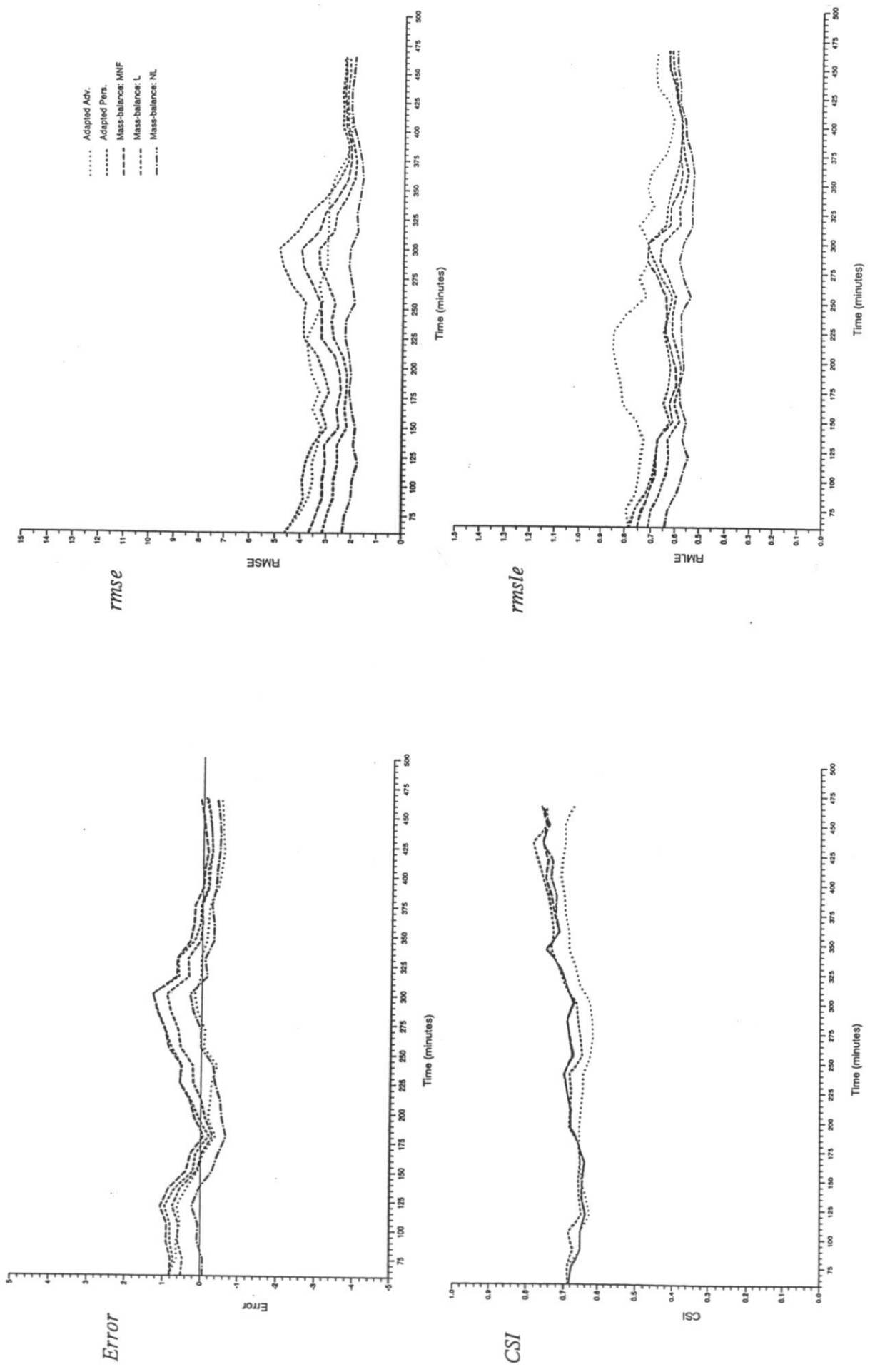
Figure 6.3.3 cont. Evolution of the one hour ahead forecast error statistics over the eight hour duration event (d) Event 4 11 June 1993
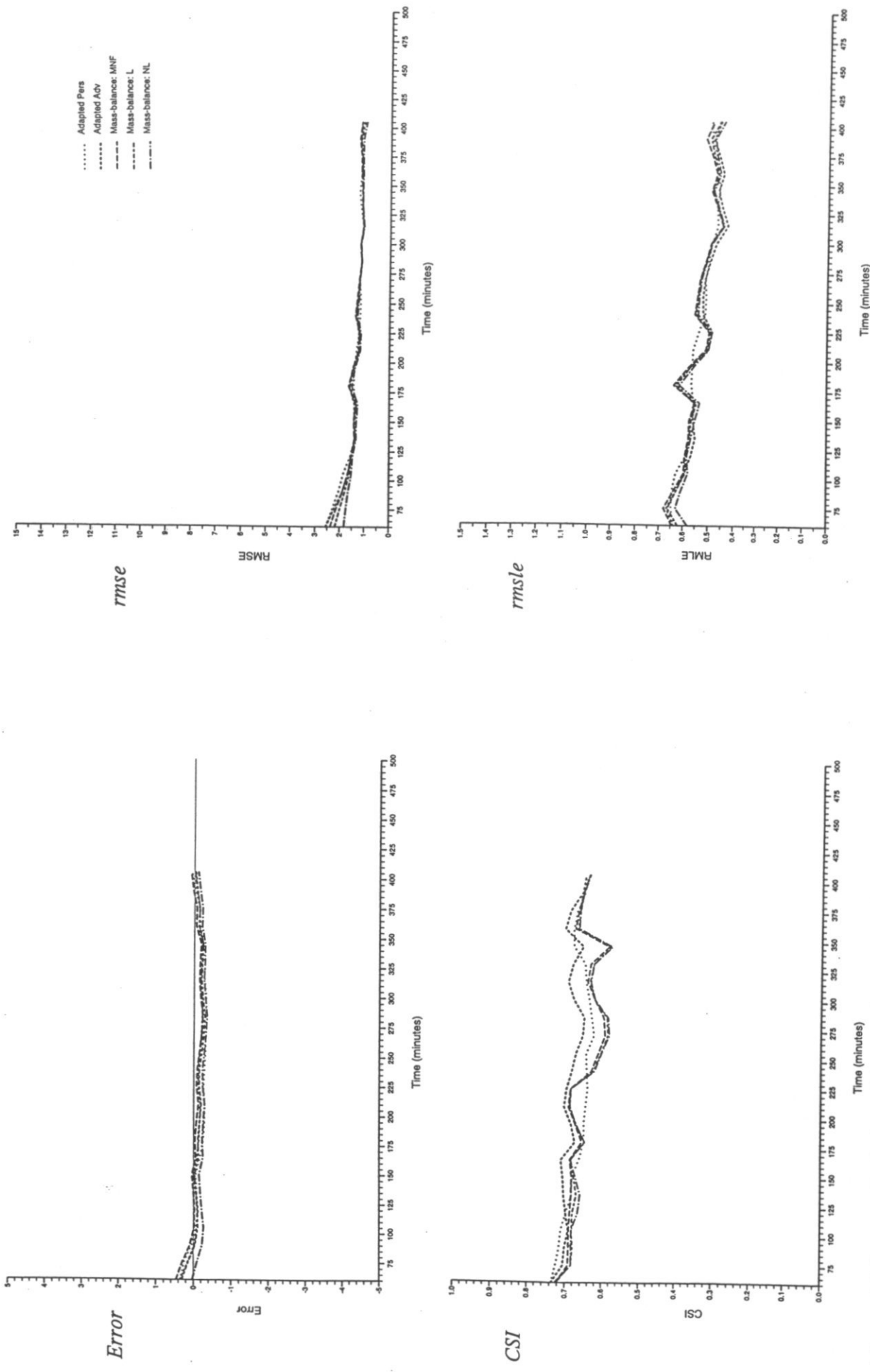
Figure 6.3.3 cont. Evolution of the one hour ahead forecast error statistics over the eight hour duration event (e) Event 5 11 June 1993
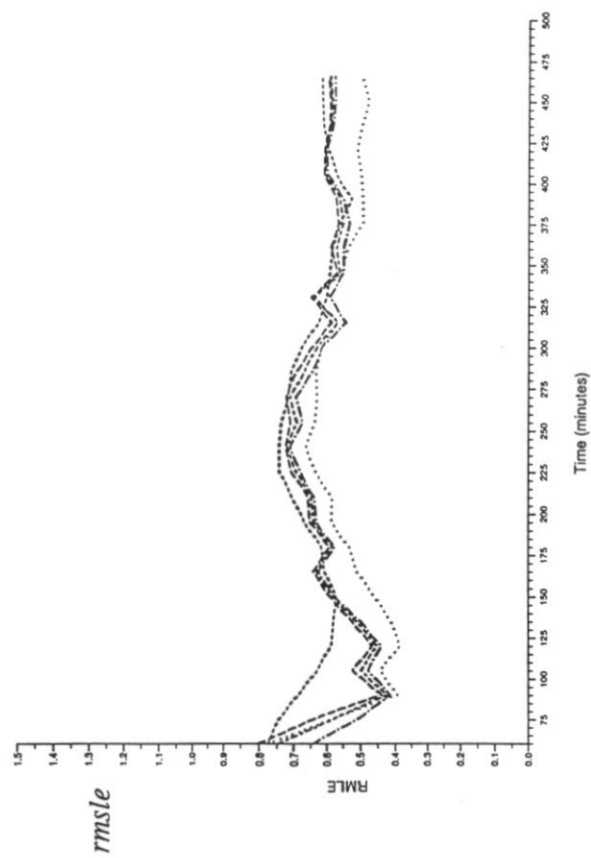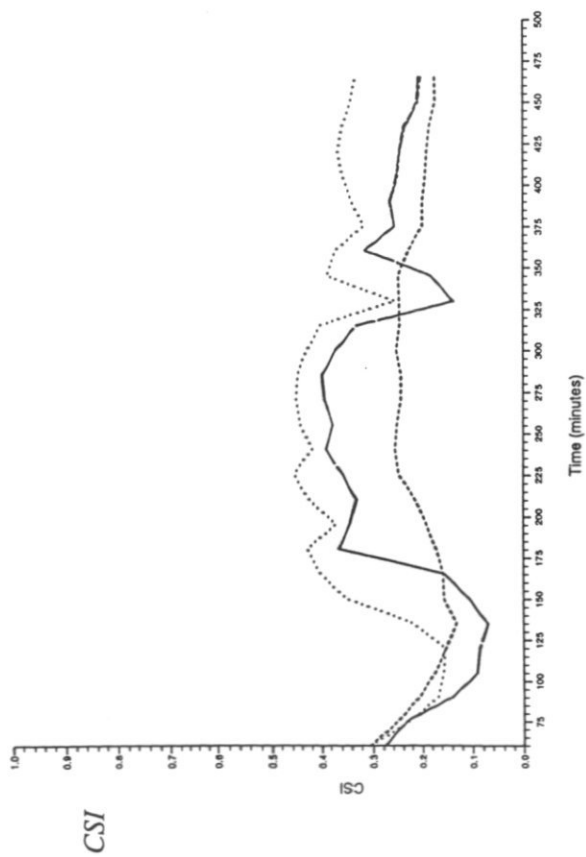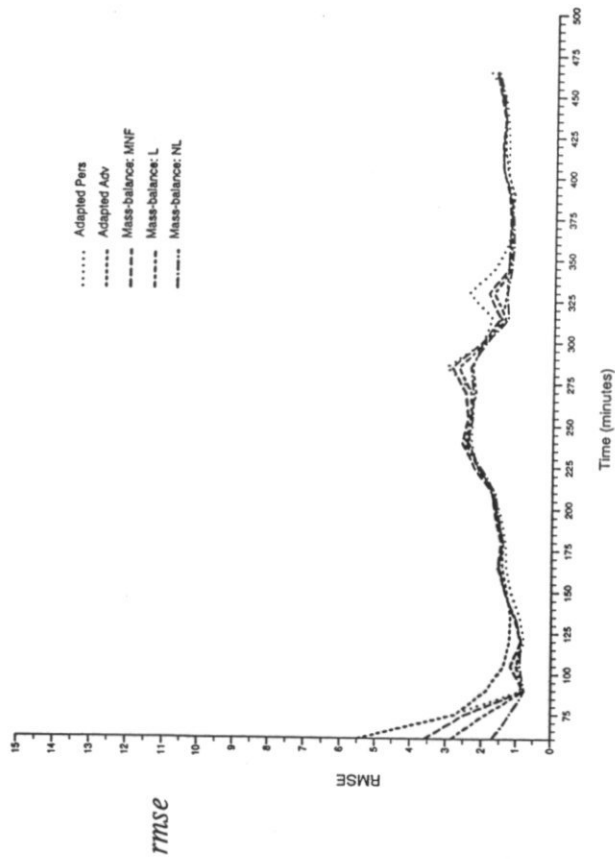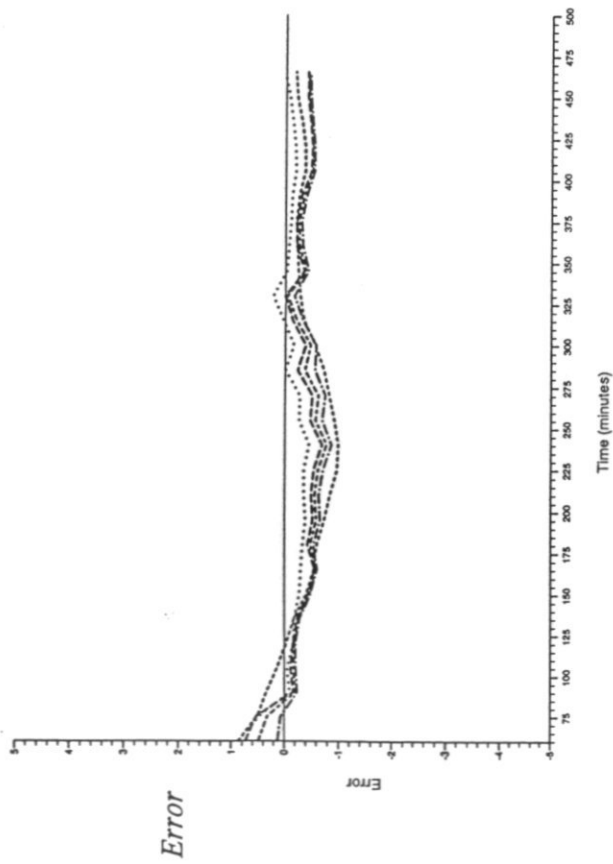
Figure 6.3.3 cont. Evolution of the one hour ahead forecast error statistics over the eight hour duration event (f) Event 6 12 June 1993

(i)   Conversion of V_L to cloud base water content (effectively rainfall in this model), M_b is achieved through the use of a fitted linear relation. Investigations have shown that the linear fit can be quite poor, sometimes leading to the physically impossible situation of a zero total cloud water, but a non-zero cloud base water content.

(ii)   The model has been shown to be sensitive to the size of the two parameters Λ_o and ϵ_o. The values used in the assessment were those suggested by French & Krajewski (1994) to be the best overall parameter set. However, these values might not necessarily be transferable to the UK and should be adjusted to provide the best model fit, perhaps with the aid of calibration.

The results show that while the model predicts the development of frontal events with some success, it is less able to predict the rapid growth and decay of convective storms. Figure 6.3.2 shows the variability of the radar-measured rain coverage in time, and the difficulty the models have in making accurate forecasts for an hour ahead.

Results support the hypothesis that the nonlinear model variant often provides the best rainfall forecasts. However, an investigation of the field maxima at each time step suggests that in the case of a convective storm, this may be due to the overestimation of the rainfall intensity which dominates the persistence/advection forecasts being reduced by the nonlinear model, leading to smaller errors. This overestimation is less likely to occur in frontal event forecasts which are, nonetheless, much improved by the use of the nonlinear model variant.

7. Summary, conclusions and suggestions for further work

7.1 SUMMARY AND CONCLUSIONS

A spatially variable rainfall forecasting model originally developed in the USA for use with 12 elevation scan radar data (French and Krajewski, 1994) has been converted for use with 4 elevation scan UK weather radar data and satellite imagery. The model incorporates components representing field advection and simple convective processes in a vertical cloud column.

The model has been successfully adapted to work with UK data, and has been restructured to allow the calculation of any number of forecasts at different lead times. A number of statistical performance measures have been introduced to facilitate model assessment.

The results obtained for the period 8 to 12 June 1993 suggest that the model is reasonably successful in forecasting frontal events, but less accurate in forecasting the development of convective storms. Five model variants have been evaluated:

(i)   Adapted-persistence where radar values are summed and converted back to rain, ignoring advection and convection processes;
(ii)   Adapted-advection is as above, but with advection included;
(iii)   Dynamic model solved by statistical linearisation;
(iv)   Dynamic model solved by 'naive' linearisation; and
(v)   Dynamic model where the full nonlinear equation is solved numerically.

The nonlinear dynamic formulation has been shown to be often superior in forecast accuracy to the adapted-advection and adapted-persistence model formulations. Results also reveal that, for convective storms in particular, the model seriously overestimates rainfall intensities, generating unrealistically large rainfall values. This is thought to be due to problems encountered in the estimation of liquid water content in each cloud column, and the conversion back to rain again.

7.2 SUGGESTIONS FOR FURTHER WORK

The work to date suggests a number of changes that might be considered for inclusion in a new version of the rainfall forecasting model. These are listed below as suggestions for further work.

(i)   An improved model performance could probably be achieved through the use of a calibration shell to optimise the two model parameters ϵ_o and Λ_o. The two parameter values used in the present assessment are those found by French & Krajewski to be the best overall set. However, they might not be applicable to the region of south-west England of concern here.

(ii)   Improvements in the estimation of V_L and rainfall might be achieved through the use of alternative methods to calculate the drop size distribution parameters, and a better

relational fit between V_L and M_b. Use of the HYREX disdrometer to support the drop size distribution parameterisation may also be of benefit.

(iii) The vertical distribution of updraft velocity can be considered to be parabolic (Kessler, 1969). The French-Krajewski model further simplifies this assumption and assumes constant updraft velocity, w_o. It might be possible instead to approximate the parabolic velocity distribution by a piecewise linear function in the manner of Georgakakos and Bras (1984a), without making the model state equations much more complicated. An orographically enhanced updraft velocity might also be considered in an extended parameterisation of the current model.

(iv) As presently implemented, the variation in the dropsize distribution parameter, Λ, with rainfall rate at the cloud base, $\Lambda = \Lambda_o \, r^{0.21}$, is inconsistent and leads to an incorrect estimate of rainfall rate at the cloud base. This should be corrected. An extension might be considered in which a different value for Λ is used in each vertical layer of the cloud column, instead of calculating a single value at the base and applying it throughout.

(v) Possible development to allow temporal changes in cloud top temperature to change the intensity of convective storms after a time lag, as observed by Adler and Fenn (1977) and Collier and Lilley (1994).

(vi) Currently model forecasts are in the form of <u>rainwater content at the cloud base</u> expressed in mm h^{-1}. Although these forecasts are consistent with the radar observations they are being compared with, it may be more appropriate to use the <u>rainfall rate</u> which is calculated in the model as part of the water balance equation for the vertical cloud column. These rainfall rate forecasts could additionally be compared with the raingauge measurements available from the Brue dense raingauge network.

(vii) Development of alternative model formulations, including alternative parameterisations of the existing mass balance equation should be considered.

(viii) Investigate the accuracy of the current advection scheme and consider the inclusion of the IH advection scheme, together with its associated radar anomaly and clutter correction procedures.

(ix) Development of a new, empirically based updating scheme to replace the Kalman filter originally present in the French-Krajewski model. For example, it might be beneficial to empirically adjust the vertically integrated cloud water content based on the knowledge of rainfall at that time, in order to take into account rainfall measurement error or deficiencies in the model.

(x) Possible development of a decision-based system to detect the nature of an event (frontal or convective, for example) based on measurements such as percentage rainfall coverage or maximum field intensity. Alternatively artificial neural networks might be used for the same task. If the type of event can be identified in this way, it would be possible to apply different model dynamics to each type of event.

(xi) Incorporation of Doppler data for use in the advection component of the model, and use of measurements of the vertical temperature variation may be beneficial. Use of

output from the mesoscale model should also be considered in this context.

(xii)   Use of full volume scan data from the new Doppler radar at Cobbacombe Cross to calculate the vertically integrated liquid water content should provide improved forecast performance and requires evaluation.

(xiii)   There is a need to further develop and evaluate the model using data for more storm events in order to obtain representative results for a range of synoptic conditions.

References

Atlas, D. & Ulbrich, C.W. 1977. Path- and area-integrated rainfall measurement by microwave attenuation in the 1-3 cm band. J. Appl. Meteorol., 16, 1322-1331.

Adler, A. & Fenn, D. 1977. Preprints, 10th Conf. on Severe Storms, 8-15. Am. Meteorol. Mag., 92: 198-210.

Brown, R., Newcomb, P.D., Cheung-Lee, J. & Ryall, G. 1994. Development and evaluation of the forecast step of the FRONTIERS short-term precipitation forecasting system. J. Hydrol., 158, 79-105.

Collier, C.G. & Lilley, R.B.E. 1994. Forecasting thunderstorm initiation in north west Europe using thermodynamic indices, satellite and radar data. Met. Apps. 1, 75-84.

French, M. N. & Krajewski, W. F. 1992. Quantitative real-time rainfall forecasting using remote sensing. IIHR Limited Distribution Report No. 200, Iowa Institute of Hydraulics Research and Department of Civil and Environmental Engineering, the University of Iowa, Iowa City, Iowa 55242, 241pp.

French, M. N. & Krajewski, W. F. 1994a. A model for real-time quantitative rainfall forecasting using remote sensing. Part 1, Formulation. Water Res. Res. Vol. 30(4), 1075-1083.

French, M. N. & Krajewski, W. F. 1994b. A model for real-time quantitative rainfall forecasting using remote sensing. Part 2, Case Studies. Water Res. Res. Vol. 30(4), 1085-1097.

Golding, B.W. 1990. The Meteorological Office mesoscale model. Meteorol. Mag., 119, 81-86.

Georgakakos, K.P. & Bras, R.L. 1984. A hydrologically useful station precipitation model, Part I, Formulation, Water Res. Res. 20(11), 1585-1596.

Georgakakos, K.P. & Bras, R.L. 1992. Real time, statistically linearised, adaptive flood routing, Water Res. Res. 18(3), 513-524.

Gun, R. & Kinser, G.P. 1949. The terminal velocity of fall for water droplets in stagnant air, J. Meteorol. 6(8), 243-248.

Hardy, R.L. 1971. Multiquadric equations of topography and other irregular surfaces. J. Geophys. Res., 76(8), 1905-1915.

Kessler, E. 1969. On the distribution and continuity of water substance in atmospheric circulation, Meteorol. Monogr., 10, 86pp.

Lancaster, P. & Šalkhauskas, K. 1986. Curve and Surface Fitting: An Introduction, Academic Press, 280 pp.

Marshall, J.S. & Palmer, W.M.K. 1948. The distribution of raindrops with size, J. Meteorol., 5, 165-166.

Moore, R.J., Hotchkiss, D.S., Jones, D.A. & Black, K.B. 1991. London Weather Radar Local Rainfall Forecasting Study: Final Report, Contract Report to NRA Thames Region, 129pp, (November 1992 update), Institute of Hydrology.

Moore, R.J., Hotchkiss, D.S., Jones, D.A. & Black, K.B. 1992. Local rainfall forecasting using weather radar: the London Case Study, Advances in Radar Hydrology, Commission of the European Communities, in press, 7 pp.

Moore, R.J., Watson, B.C., Jones, D.A. & Black, K.B. 1989. London weather radar local calibration study: final report. Contract report to the National Rivers Authority Thames Region, 85pp, Institute of Hydrology.

Moore, R.J., May, B.C., Jones, D.A. & Black, K.B. 1991. Local calibration of weather radar over London, Advances in Radar Hydrology, Commission of the European Communities, in press, 10pp.

Press, Flannery, Tenkolsky & Vetterling. 1989. Numerical Recipes, the Art of Scientific Computing, 674 pp, C.V.P. New York.

Rogers, R.R. & Yau, M.K. 1989. A short course in cloud physics, 3rd ed. 293 pp. Pergamon, New York.

Seo, D.J. & Smith, J.A. 1992. Radar-based short-term rainfall prediction, J. Hydrol., 131, 341-367.

Sulakvelidze, G.K. 1969. Rainstorms and hail. Israel Program for Scientific Translations, Jerusalem.

Smolarkiewicz, P.K. & Clark, T.L. 1985. Numerical simulation of the evolution of a three dimensional field of cumulus clouds. Part I: Model description, comparison with observations and sensitivity studies. J. Atmos. Sci. 42, 502-522.

Wallace, J.M. & Hobbs, P.V. 1977. Atmospheric Science. An Introductory Survey, 467pp. Academic, San Diego, Calif.

Appendix I Derivation of the equation for velocity of rainwater at the cloud base

The velocity of rainwater at the cloud base

$$v_b = W_T - w_o \qquad (I.1)$$

where W_T is the free fall velocity of rain water in still air and w_o is the vertical velocity of air. The parameterisation for v_b used in the French-Krajewski model is

$$v_b = \Lambda^{-\beta} \frac{\alpha}{6} \Gamma(4+\beta) - w_o = \{M_b/(\pi \rho_o N_o)\}^\gamma \frac{\alpha}{6} \Gamma(4+\beta) - w_o \qquad (I.2)$$

where M_b is the liquid water content at the cloud base, ρ_o is water density, Λ and N_o are parameters in the dropsize distribution, α and $\gamma = \beta/4$ are empirical dimensionless parameters in the formula for raindrop terminal velocity and $\Gamma(\ )$ is the gamma function.

The derivation of the parameterisation (I.2) from (I.1) is as follows. Given v_b is the rainwater velocity and M_b is the liquid water content at the cloud base, it follows that rainfall rate at the cloud base is

$$R_b = \frac{1}{\rho_o} M_b v_b \qquad (I.3)$$

where ρ_o is the density of water. If we can find independent expressions for R_b and M_b then (I.3) can be used to derive an expression for v_b.

The rain rate is related to the rain drop diameter, D, and the rain drop size distribution, N(D), according to (Doviak and Zrnić, 1984)

$$R_b = \frac{\pi}{6} \int_o^\infty D^3 N(D) \, v_b dD \ . \qquad (I.4)$$

Following Marshall and Palmer (1948) the drop concentration is assumed to decrease exponentially with increasing diameter according to the expression

$$N(D) = N_o \exp(-\Lambda D) \qquad (I.5)$$

where N_o and Λ are parameters.

The raindrop terminal velocity, W_T, is assumed to follow the empirical formula of Atlas and Ulbrich (1977):

$$W_T = \alpha D^\beta \ . \qquad (I.6)$$

If W_T and D have units m s⁻¹ and m respectively, then values for the parameters, based on the data of Gunn and Kinzer (1949), are $\alpha = 386.6$ m$^{1-\beta}$ s⁻¹ and $\beta = 0.67$ for

43

.0005 < D < .005 m.

Substituting (I.5), (I.1) and (I.6) into (I.4) gives

$$R_b = \frac{\pi}{6} \int_0^\infty D^3 N_o e^{-\Lambda D}(\alpha D^\beta - w_o)\, dD$$

$$= \frac{\pi}{6} N_o \left[\alpha \int_0^\infty D^{3+\beta} e^{-\Lambda D}\, dD - w_o \int_0^\infty D^3 e^{-\Lambda D}\, dD \right]$$

(I.4)

Using the standard definite integral $\int_0^\infty x^n e^{-ax}\, dx = \Gamma(n+1)/a^{n+1}$, where $\Gamma(n+1)$ is the gamma function which for integer n equals n!, gives the result

$$R_b = \frac{\pi}{6} N_o \Lambda^{-4}\left(\alpha \Lambda^{-\beta} \Gamma(4+\beta) - w_o \Gamma(4)\right).$$

(I.7)

The liquid water content at the cloud base is given by (Doviak and Zrnić, 1984, p.189)

$$M_b = \frac{\pi}{6}\rho_o \int_0^\infty D^3 N(D)\, dD = \frac{\pi}{6}\rho_o N_o \int_0^\infty D^3 e^{-\Lambda D}\, dD$$

$$= \pi \rho_o N_o \Lambda^{-4} .$$

(I.8)

Substituting this along with (I.7) into (I.3) gives the required expression for the velocity of rain water at the cloud base:

$$v_b = \frac{\alpha}{6}\Lambda^{-\beta}\Gamma(4+\beta) = w_o \left\{M_b/(\pi \rho_o N_o)\right\}^\gamma \frac{\alpha}{6}\Gamma(4+\beta) - w_o .$$

(I.2)

Appendix II Derivation of Parcel Theory equations

Poisson's equation (Wallace and Hobbs, 1977, p.69) is

$$\theta = T\left[\frac{p_n}{p}\right]^{\kappa} . \tag{II.1}$$

The quantity θ is the potential temperature of a parcel of air defined as the temperature of the parcel if it were expanded or compressed adiabatically (without heat exchange) from its existing pressure and temperature, p and T, to a standard pressure, p_n, generally taken to be 1000 mb. Exponent κ is the ratio of the specific constant, R_d, to the specific heat capacity, c_p, for dry air. Specifically $\kappa = R_d/c_p = 287/1004 = 0.286$.

The equivalent potential temperature θ_e of an air parcel is the potential temperature when its saturation mixing ratio r_s is zero and is given by (Wallace and Hobbs, 1977, p.79) as

$$\theta_e = \theta \exp\left[\frac{Lr_s}{c_p T}\right] . \tag{II.2}$$

We therefore have

$$\theta_e = T\left[\frac{p_n}{p}\right]^{\kappa} \exp\left[\frac{Lr_s}{c_p T}\right] . \tag{II.3}$$

A derivation of (II.2) follows from the First Law of Thermodynamics, the Ideal Gas equation and Poisson's equation as follows. The First Law of Thermodynamics may be stated as

$$dq = c_p dT - \alpha dp \tag{II.4}$$

where q is heat, T is temperature and p is pressure, c_p is the specific heat at constant pressure $(=(dq/dT)_{p\,const})$ and α is the specific volume of the gas (or the volume occupied by unit mass). The Ideal Gas equation for unit mass (1 kg) of gas is

$$p\alpha = RT \tag{II.5}$$

where R is the gas constant. Dividing the equation for the First Law of Thermodynamics by T and introducing the specific gas ratio $\kappa = R/c_p$ gives

$$\frac{1}{c_p}\frac{dq}{dT} = \frac{dT}{T} - \kappa\frac{dp}{p} . \tag{II.6}$$

Taking logarithms of Poisson's equation and differentiating with respect to T gives

$$\frac{d\theta}{\theta} = \frac{dT}{T} - \kappa\frac{dp}{p} . \tag{II.7}$$

Combining this with the previous equation gives

$$\frac{d\theta}{\theta} = \frac{1}{c_p}\frac{dq}{T} \; . \tag{II.8}$$

Now, if r_s is the saturation mixing ratio of air and water, the heat exchange with a unit mass of dry air due to condensation (or evaporation) of liquid water is $dq = - L \, dr_s$, where L is the latent heat of condensation. Substituting this into the above and noting the approximation

$$\frac{L}{c_p T} \, dr_s = d\left[\frac{L r_s}{c_p T}\right]$$

gives

$$\frac{d\theta}{\theta} = -d\left[\frac{L r_s}{c_p T}\right] \; .$$

Integrating this with a lower limit θ_e when $r_s/T\rightarrow0$ gives the result

$$\theta_e = \theta \, \exp\left[\frac{L r_s}{c_p T}\right] \; . \tag{II.3}$$

Finally, derivation of Poisson's equation for potential temperature, equation II.1, follows again from the First Law of Thermodynamics and the Ideal Gas equation. Since this concerns the temperature of a parcel of air undergoing adiabatic expansion from a pressure and temperature, p and T, to a standard pressure, p_n, then $dq = 0$ in equation (II.4) for the First Law of Thermodynamics. Combining this with the Ideal Gas equation (II.5) gives

$$\kappa \frac{dT}{T} = \frac{dp}{p} \; . \tag{II.9}$$

Integrating with a lower limit p_n when $T = \theta$ gives the result

$$\theta = T\left[\frac{p_n}{p}\right]^\kappa \; . \tag{II.1}$$

Now consider a moist but unsaturated parcel of air near the ground with pressure, temperature and dew point temperature denoted by p_0, T_0 and T_d. As the parcel ascends and cools the saturation vapour pressure, e_s, decreases. Rogers and Yau (1989, p14) give an approximation expression for e_s at a temperature T as

$$e_s(T) = A \, \exp(-B/T) \tag{II.10}$$

where $B = 5420°K$ and A is a known constant. The mass of water vapour per unit mass of dry air is referred to as the initial mixing ratio, r_0, and is defined with reference to the saturation mixing ratio, $r_s(T_d, p_0)$, as

$$r_o = r_s(T_d, p_o) = \epsilon \frac{e_s(T_d)}{p_o - e_s(T_d)} \simeq \epsilon \frac{e_s(T_d)}{p_o} \tag{II.11}$$

where ϵ is a known constant. The approximation derives from the fact that $p_o >> e_s(T_d)$. Now the parcel of air will ascend adiabatically with constant potential temperature, θ, up to the lifting condensation level, LCL, at which saturation occurs. During its ascent cooling occurs according to the Poisson equation

$$T + \theta \left[\frac{p}{p_n} \right]^\epsilon . \tag{II.12}$$

Combining this with (II.10) and (II.11) gives

$$r_o = \frac{A_o}{p_o} \exp(-B/T_d) \tag{II.13}$$

where $A_o = \epsilon A$. It also follows from this that the saturation mixing ratio

$$r_s(T_o, p_o) = \frac{A_o}{p_o} \exp(-B/T_o) . \tag{II.14}$$

At the lifting condensation level let the temperature and pressure be denoted as T_s and p_s respectively. Since the temperature T_s will be the dew point temperature, then the form of equation (II.13) gives this temperature as

$$T_s = \frac{B}{\ln\{A_o/(r_o p_s)\}} . \tag{II.15}$$

Substituting (II.13) for r_o into this gives

$$T_s = \frac{BT_d}{B + T_d \ln(p_o/p_s)} . \tag{II.16}$$

Poisson's equation applied near the surface gives

$$\theta = T_o \left[\frac{p_n}{p_o} \right]^\epsilon \tag{II.17}$$

which can be substituted in Poisson's equation (II.12) applied at the LCL to give an alternative expression for T_s, as

$$T_s = T_o \left[\frac{p_o}{p_s} \right]^\epsilon . \tag{II.18}$$

Thus,

$$T_o \left[\frac{p_o}{p_s} \right]^{\varkappa} = \frac{B T_d}{B + T_d \ln(p_o/p_s)} \qquad \text{(II.19)}$$

can be solved for p_o/p_s, given surface observations of T_o and T_d, and then used to calculate p_s and T_s at the LCL (French and Krajewski, 1992). Brent's method of root finding is used in practice in the solution of (II.19) (Press *et al.*, 1989).

Above the LCL condensation occurs to form the liquid water content of the cloud and the parcel of air is warmed by the release of the latent heat of condensation. The parcel rises pseudo-adiabatically with constant equivalent potential temperature, θ_e, given by (II.3). The quantity θ_e can be evaluated at the LCL using the p_s and T_s values calculated above. Applying the same equation at the cloud top level, and using this value of θ_e and the satellite-inferred cloud top temperature, T_t, allows the pressure, p_t, at the cloud top to the determined, again using Brent's method. In this way the level of maximum ascent of the air parcel is established.

48

Appendix III Calculation of liquid water content and vertically integrated liquid water content from radar data

The rainfall forecasting model defines the space-time evolution of the vertically integrated liquid water content, V. In order to assess the model, and to initialise and update the model for forecasting purposes, observations of V are required. In addition to V, the "measured" liquid water content M is used to calculate the regression parameters a and b at each time step, relating M_bH to V. V and M are estimated from multi-scan radar data as follows.

The radar reflectivity, Z, is the integral of the drop diameter, D, to the sixth power of all drops in a unit volume, so

$$Z = \int_o^\infty D^6 N(D) dD \qquad \text{(III.1)}$$

where N(D) is the drop size distribution. Assuming the Marshall-Palmer exponential drop size distribution

$$N(D) = N_o \exp(-\wedge D), \qquad \text{(III.2)}$$

where N_o and $\wedge$ are the drop size distribution parameters, then

$$Z = 720 N_o \wedge^{-7} ; \qquad \text{(III.3)}$$

note 720 = 6!. Solving for N_o gives

$$N_o = \frac{\wedge^7}{720} Z . \qquad \text{(III.4)}$$

The Liquid Water Content is given by (see Appendix II)

$$M = \pi \rho_o N_o \wedge^{-4} \qquad \text{(III.5)}$$

so combining (III.4) and (III.5) gives a relation between liquid water content and radar reflectivity as

$$M = \frac{\pi \rho_o \wedge^3}{720} Z \qquad \text{(III.6)}$$

and leaving $\wedge$ as the drop size parameter to be estimated.

Given multi-scan radar data these can be used to estimate the vertically integrated liquid water content, V, using the discrete summation of M (calculated from Z using (III.6)) values for n_z different elevation scans between the bottom and top of the radar echoes:

$$V = \sum_{i=1}^{n_z} M(z_i)\Delta h_i \tag{III.7}$$

where Δh_i is the height increment to be associated with the i'th radar scan elevation. French & Krajewski used this scheme because they had volume scan data incorporating 12 scan elevations. In the present study using UK data, with only values for four elevation scans, an interpolation scheme is used to map radar data onto 15 points in the vertical at equal height increments of 1 km (see Appendix V); thus $\Delta h_i = 1$ for all i with $n_z = 15$.

Appendix IV Statistics used in assessing model performance

The performance of a rainfall forecast can be assessed with reference to absolute quantities or in terms of the skill to forecast rain or no-rain, without regard to magnitude. In the latter case the observed and forecast data for each radar pixel and time-period are considered reduced to the categories "rain" and "no-rain". A two-way correspondence table is calculated with entries giving the number of joint occurrences between the observed and forecast categorised fields. Table IV.1 shows such a correspondence table.

Table IV.1 Two-way contingency table for categorical assessment of forecast performance

	Forecast		
Observed	rain	no rain	
rain	n_{11}	n_{12}	$n_{11} + n_{12}$
no rain	n_{21}	n_{22}	$n_{21} + n_{22}$
	$n_{11} + n_{21}$	$n_{12} + n_{22}$	

Measures of the skill of the forecast can then be formulated based on this correspondence table. The following categorical skill indices have been considered here:

Critical Success Index

$$CSI = \frac{n_{11}}{n_{11} + n_{12} + n_{21}} \tag{IV.1}$$

False Alarm Rate

$$FAR = \frac{n_{12}}{n_{11} + n_{12}} \tag{IV.2}$$

Probability of Detection

$$POD = \frac{n_{11}}{n_{11} + n_{21}} \, . \tag{IV.3}$$

As a measure of association between a forecast and observed rainfall field which considers rainfall magnitude, the correlation coefficient might seem an obvious choice. However, a high correlation does not necessarily imply that observed and forecast rainfall fields will be approximately equal and, as a consequence, correlation is not used here as a performance measure. The main criteria used is the root mean square error, or rmse, defined as

$$\text{rmse} = \left(n^{-1} \Sigma \; e_i^2\right)^{\frac{1}{2}} \tag{IV.4}$$

where ϵ_i is the forecast error between the forecast and observed rainfall, $\hat{R}_i$ and R_i, such that

$$\epsilon_i = R_i - \hat{R}_i \; . \tag{IV.5}$$

The summation is computed over n values, pooled over each radar pixel and time frame for the forecast of interest.

A variant on the rmse, referred to as the root mean square log error or rmsle, employs the log error

$$e_i^{'} = \ln \left[\frac{1 + R_i}{1 + \hat{R}_i} \right] \tag{IV.6}$$

in place of e_i in (IV.4). This performance criteria deflates the influence of a large error when the rainfall rate is high.

A further performance measure, related to rmse, used here is the R^2 goodness-of-fit statistic

$$R^2 = 1 - \frac{\Sigma \epsilon_i^2}{\Sigma (R_i - \bar{R})^2} \tag{IV.7}$$

where $\bar{R}$ is the mean of the observations over the n values. This gives the proportion of the variance in the observations accounted for by the forecast, and provides a measure of performance relative to a naive forecast based on the (unknown in real-time) mean rainfall.

Finally, as a measure of forecast bias the mean error

$$\bar{\epsilon} = n^{-1} \Sigma \; \epsilon_i \tag{IV.8}$$

is also calculated.

Appendix V Multiquadric interpolation

The problem of mapping an irregular spaced set of values in two- or three-dimensional space into a regular spaced set is essentially one of interpolation. In two-dimensions fitting a mathematical surface to the values and using the surface as an interpolant provides a direct and simple approach, and one which can be extended to three-dimensions. Moore *et al.* (1989, 1991), extending the work of Hardy (1971), propose new methods of fitting multiquadric surfaces subject to constraints which are both physically appealing and computationally efficient. The theory of one of these methods is presented here which has been found appropriate for the interpolation of multi-scan radar, surface climate, Meteosat cloud top temperature and radiosonde data. This includes development of the method for use in three-dimensional interpolation.

Let z_i be the values observed at n locations, having spatial coordinates $\underline{x}_i = (u_i, v_i)$. The multiquadric surface is defined as the weighted sum of n distance, or basis functions centred on each observation location; that is

$$s(\underline{x}) = \sum_{j=1}^{n} a_j \, g(\underline{x} - \underline{x}_j) + a_0 \qquad\qquad\qquad (V.1)$$

where $\{a_j, \, j = 0, 1, 2, \ldots, n\}$ are parameters of the surface. The distance function used here is the exponential distance function

$$g(\underline{x}) = \exp(- \|\underline{x}\| / \ell) \qquad\qquad\qquad (V.2)$$

where $\|\underline{x}\|$ is the Euclidean distance

$$\|\underline{x}\| = \sqrt{(u^2 + v^2)} \ . \qquad\qquad\qquad (V.3)$$

and ℓ is a scaling length parameter. This exponential form of distance function is sometimes referred to as rotated Gaussian (Lancaster and Šalkauskas, 1986, p.255).

Formally, estimation of the a_j weights is achieved as follows. Equation (V.1) for

$$s(\underline{x}_i) = \sum_{j=1}^{n} a_j \, g(\underline{x}_i - \underline{x}_j) + a_0 = z_i \qquad\qquad (i = 1, 2, \ldots, n) \qquad\qquad (V.4)$$

may be expressed in matrix form as

$$\underline{G}\,\underline{a} + a_0 \underline{1} = \underline{z} \qquad\qquad\qquad (V.5)$$

where $\underline{G}$ is an n by n matrix with the (i,j)'th element given by $G_{ij} = g(\underline{x}_i - \underline{x}_j)$, $\underline{1}$ is a unit vector of order n, and $\underline{z}$ is the vector containing the n observation values. As one approach to avoiding anomalies in the surface form away from the n observation points, an additional requirement for flatness at large distances is imposed through the constraint

$$\underline{a}^T \underline{1} = 0. \qquad\qquad\qquad (V.6)$$

For the exponential distance function this constraint corresponds to a requirement of zero-

slope with increasing distance from the set of observation points. Solution of equation (V.5) subject to constraint (V.6) for the weighting coefficients gives

$$a_0 = (\underline{1}^T \underline{G}^{-1} \underline{z})/(\underline{1}^T \underline{G}^{-1} \underline{1}) \tag{V.7}$$

$$\underline{a} = \underline{G}^{-1}(\underline{z} - a_0 \underline{1}) . \tag{V.8}$$

In order to deflate the effect of variability at high rainfall rates on the form of the fitted surface a further variant of the method employs a logarithmic transform of the observation values for the observation vector $\underline{z}$. The particular transform used is that introduced by Moore *et al.* (1989) for interpolating rainfall fields from raingauge data. This has the form

$$z = \begin{cases} R/R_o + \log(R_o) - 1 & 0 \le R \le R_o \\ \log R & R > R_o \end{cases} \tag{V.9}$$

where R is the observation value and R_o is a threshold parameter. In the case of gauge rainfall measured in mm h^{-1} a value of 4.5 has been found appropriate. Any negative values of interpolated R values, resulting from back-transformation, are replaced by zero.

The multiquadric interpolation method naturally extends to three-dimensional interpolation through replacing the two-dimensional Euclidean distance measure (V.3) by the equivalent in three dimensions

$$\| \underline{x} \| = \sqrt{u^2 + v^2 + w^2} \tag{V.10}$$

where the observation points now have spatial co-ordinates $\underline{x}_i = (u_i, v_i, w_i)$ with w_i referring to the vertical dimension. Note also that the multiquadric interpolation for one dimension is simply a special case, with both (V.3) and (V.10) being applicable.

The application of the multiquadric interpolation method to the meteorological data fields involved in this study are outlined below for each data type.

Weather radar data

Weather radar data are used at a 15 minute sampling interval, available for a 210 km radius circle within an 84 by 84 5 km grid area for beam elevations of 0.5°, 1.5°, 2.5° and 4°. Three-dimensional multiquadric interpolation is employed to map these onto a regular 84 by 84, 5 km grid in the horizontal and 15, 1 km intervals in the vertical. The log-transform defined by (V.9) is used along with a scaling length parameter of 20 km in the exponential distance function. Interpolation of the 15 points in the vertical for a given 5 km radar pixel column employs the four observation values for the column and those for the four columns 10 km to the east, west, north and south (Figure V.1). This restricts the number of observation values to a maximum of 20, four for each of the 5 columns, when interpolating for a given 1 km height increment in the column. The interpolation is as a consequence not too computer intensive.

The basic interpolation scheme is such that rainfall will tend to zero with increasing distance from the points. Since in the vertical rainfall will tend towards zero at the top of the troposphere a variant of the scheme has been used which introduces a slight attenuation with height after interpolation. If $\dot{R}$ is the interpolated value of radar rainfall at the point (i,j,k) then an attenuated interpolated rainfall is calculated as
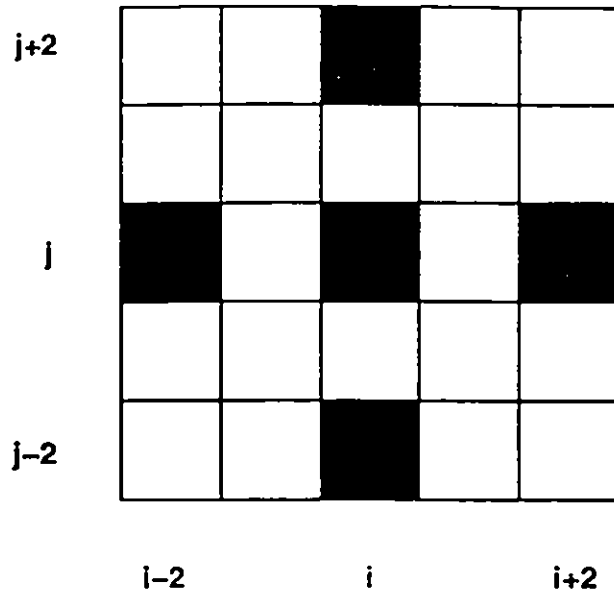
Figure V.1 Horizontal slice through the radar pixel column to be interpolated and the neighbouring pixel columns; those shown in black are included in the interpolation.

$$\hat{R}_a = f\hat{R} \qquad (V.11)$$

where the attenuation factor f is given by

$$f = a^{b^r} \qquad (V.12)$$

where a = 0.99984 and b = 0.25, when rainfall has units mm h^{-1}.

Meteosat data

The Meteosat cloud top temperature data, at 30 or 60 minute intervals, are on a regular grid when considered on a polar-stereographic projection but when transformed to a national grid projection are irregularly spaced. A two-dimensional multiquadric interpolant is used with log-transformed observations and a scaling length parameter equal to 20 km in the exponential distance function. Only observation points within 15 km of the interpolated pixel are used. The interpolated field extends over the same 210 km radius circle within the 84 by 84 5 km area as defined for the weather radar data.

Surface climate station data

The model requires instantaneous values of air temperature, dew point temperature and air pressure from surface observing stations. These data are available from the Synoptic Data Bank at hourly intervals for 15 stations identified across southern England and Wales. These data have been mapped onto the same 84 by 84, 5 km grid as used by the weather radar using

55

the two-dimensional multiquadric interpolation method with log-transformed observations and an exponential distance function. The scaling length in this case has been increased from the normal 20 km to 200 km to reflect the greater spread of observation points.

Radiosonde data

These data are not currently used within the model but have been visualised to support the interpolation of model results and to investigate model parameterisations. Radiosonde ascents are made at varying time intervals depending on the site, time of day and day of the week. For example, at Herstmonceux the most frequent and regular ascents are made at 6 hour intervals, whilst at Larkhill and Camborne the frequency varies from 7 to 18 hours and from 11 to 13 hours respectively.

Data for a given site for successive ascents allows the construction of height-time fields of the radiosonde measured quantities. The fields have been obtained using the two-dimensional multiquadric method but with the Euclidean distance now relating to a position in time and vertical height i.e. $x_i = (t_i, w_i)$. Again the exponential distance function is used with a scaling length equal to 20 km. Equation (V.9) is employed to transform the observation values. A regular grid in time and height is defined and the observation values mapped onto this by multiquadric interpolation. This has been done for the Herstmonceux data using values at points which lie within 8 hours in the horizontal and 4 km in the vertical of the interpolant point. The displayed fields are essentially two-dimensional time series plots.

Appendix VI Investigation of the presence of solid precipitation in the storm events used for model assessment

The possible existence of solid forms of water in the atmospheric column - as hail, snow or graupel - are not considered in the cloud water balance model or in the radar equations linking radar reflectivity to rain rate. If solid forms of precipitation are present this can be a major reason for the model to fail or for the radar-inferred "rain rates" to be misleading. For example, it is well known that the effect of a radar beam passing through melting precipitation produces an anomalously high electromagnetic return signal called the "bright band" which when used in the standard Z-R relation can give a gross overestimate of the rain rate at the ground. The term "bright band" stems from the characteristic annular or band of high reflectivity produced when the inclined radar beam intersects the freezing layer during conditions of precipitation formation. For this reason, investigations have been made to establish whether solid precipitation is likely to be significant over the period 8 to 12 June 1993 used for model assessment purposes.

The presence of solid precipitation has been investigated using both multi-scan radar data and radiosonde data. An initial analysis based on daily average radar image displays suggested little evidence of bright band for the period 8 to 10 June 1993, when weather conditions were fairly mild. The 8th was fairly dry in any case whilst showers on the 9th and 10th failed to yield a clear bright band signature. However, on the 11th and 12th during more frontal rain bright band is apparent, especially in the 2.5° and 4° elevation scans (Figure VI.1). Conditions on these two days have been examined in greater detail using 3 and 6 hour average radar rainfall image displays together with radiosonde data. An example of a 3 hour display for 18:00 to 21:00 on 11 June for the 4° beam is shown in Figure VI.2: the annular ring corresponds to a height range of 2.3 to 4.6 km. An analysis of the radiosonde data for Larkhill (Grid reference: 414 145) at 06:00 on the same day gives elevations for the 273 and 268°K isotherms as 2.8 and 3.8 km respectively. Radiosonde data for 23.00 on the same day at Camborne gives corresponding heights of 2 and 4.1 km. The radiosonde data therefore broadly confirm the presence of a melting layer giving rise to the bright band seen in Figure VI.2. An east-west vertical transect through the six hour average radar data for the period 18:00 to 23:55 11 June, obtained by vertical multiquadric interpolation, also suggests the presence of bright band (Figure VI.3).

Six hour average radar image fields for the 4° elevation scan on 12 June 1993 again expose the presence of bright band in the first 6 hours, but not later on. The elevation of the bright band is in the range 3.4 to 4.6 km, whilst the Camborne radiosonde data for 11.00 give the 273 and 268°K isotherm levels as 3 and 3.8 km respectively.

These results suggest that the frontal events 3, 4 and 5 may be affected by solid precipitation, particularly event 5 later on in the day. The mixed frontal/convective event on 12 June is somewhat later than the main bright band activity seen in the first 6 hours of the day. Bright band is not clearly apparent during the convective events 1 and 2 on the 9th and 10th when weather conditions were showery but mild. However, it is possible that solid precipitation was present inside the intense convective cells that were present in the field at this time.
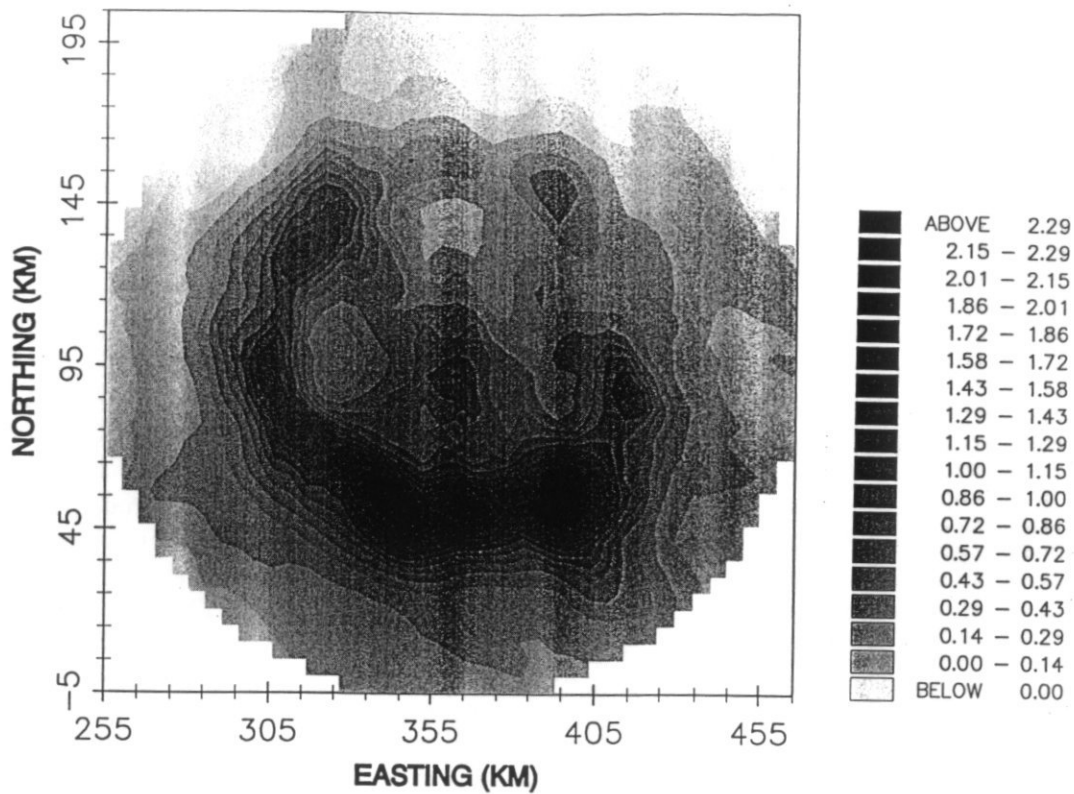
Figure VI.1 *Daily average radar rainfall field for Wardon Hill radar: 11 June 1993, 4° beam elevation*
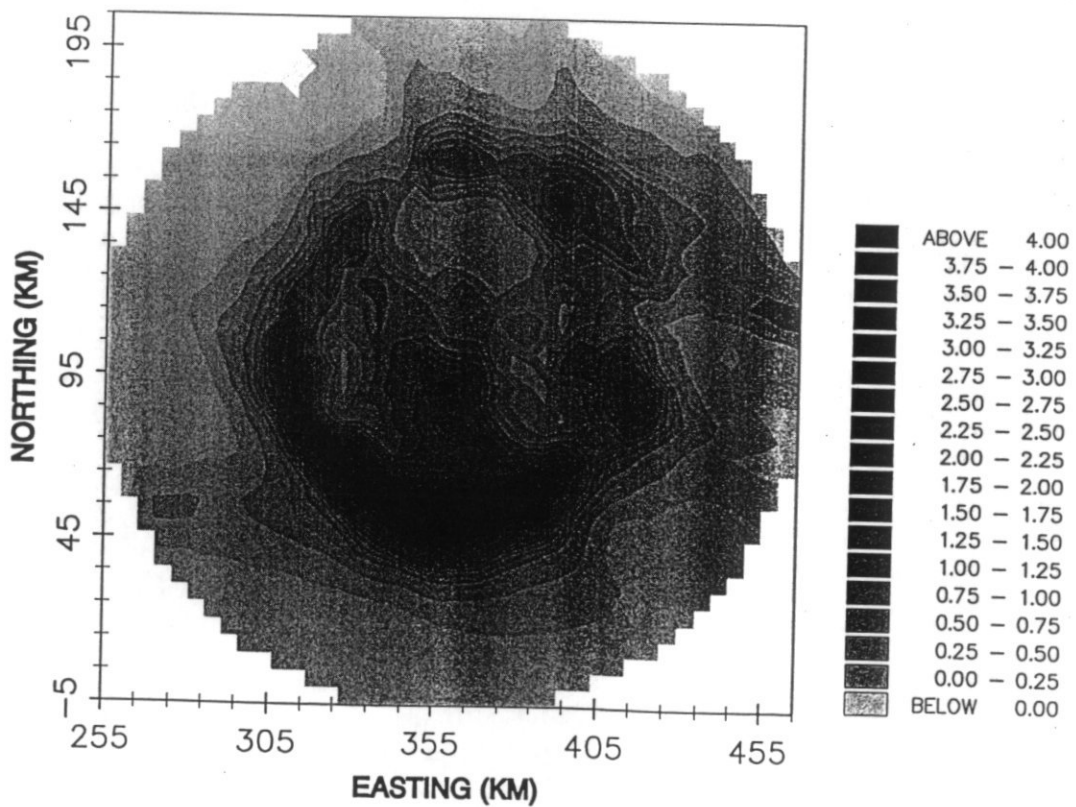

Figure VI.2 *3 hour average radar rainfall field for Wardon Hill radar: 18:00 to 21:00 11 June 1993, 4° beam elevation*
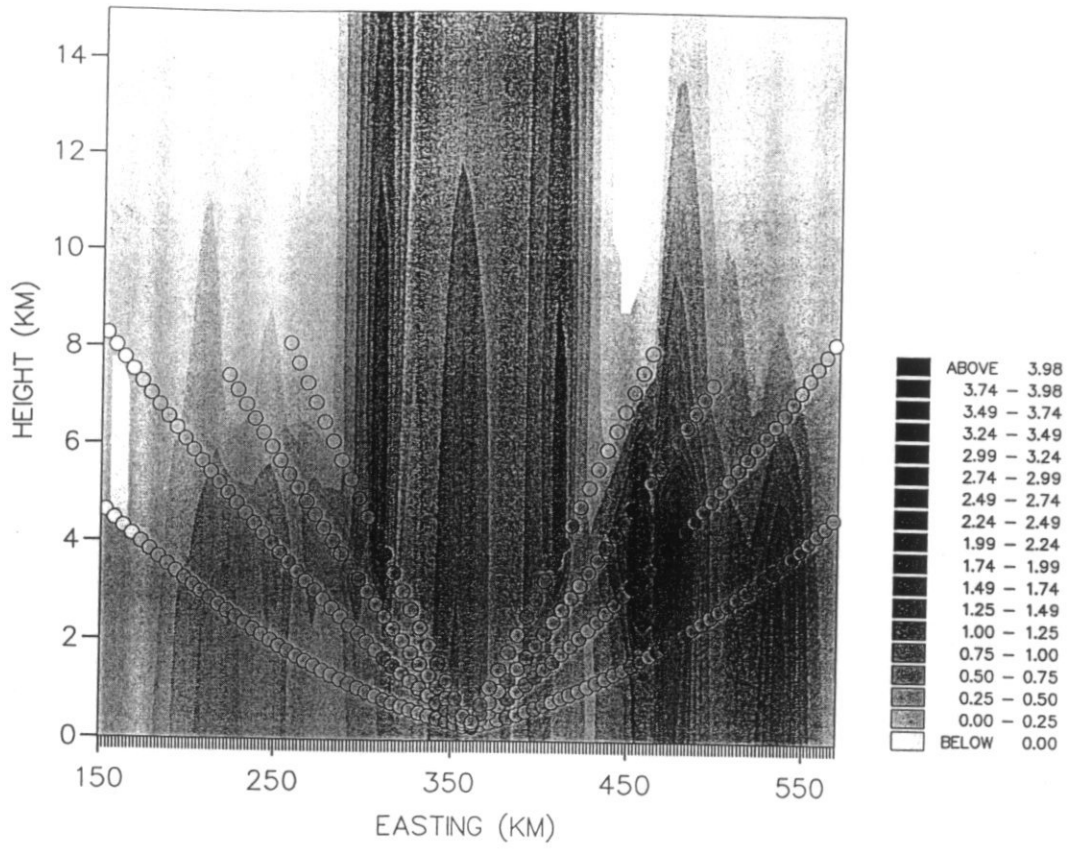
Figure VI.3 *East-west vertical transect through 100 km northing for interpolated 6 hour average radar rainfall field: Wardon Hill radar 18:00 to 23:55 11 June 1993*